HHS Public Access

Author manuscript

Cell Rep. Author manuscript; available in PMC 2023 January 18.

Published in final edited form as:

Cell Rep. 2022 December 27; 41(13): 111880. doi:10.1016/j.celrep.2022.111880.

Secreted phosphoprotein 1 slows neurodegeneration and rescues visual function in mouse models of aging and glaucoma

Song Li[1,2,*], **Tatjana C. Jakobs**[1,2,3,*]

[1]Department of Ophthalmology, Harvard Medical School, Boston, MA 02114, USA

[2]Schepens Eye Research Institute, Massachusetts Eye and Ear, Boston, MA 02114, USA

[3]Lead contact

SUMMARY

Aging causes an irreversible, cumulative decline in neuronal function. Using the visual system as a model, we show that astrocytes play a critical role in maintaining retinal ganglion cell health and that deletion of SPP1 (secreted phosphoprotein 1, or osteopontin) from astrocytes leads to increased vulnerability of ganglion cells to age, elevated intraocular pressure, and traumatic optic nerve damage. Overexpression of SPP1 slows the age-related decline in ganglion cell numbers and is highly protective of visual function in a mouse model of glaucoma. SPP1 acts by promoting phagocytosis and secretion of neurotrophic factors while inhibiting production of neurotoxic and pro-inflammatory factors. SPP1 up-regulates transcription of genes related to oxidative phosphorylation, functionally enhances mitochondrial respiration, and promotes the integrity of mitochondrial microstructure. SPP1 increases intracellular ATP concentration via up-regulation of VDAC1.

In brief

Li and Jakobs report that Spp1 knockout mice are more susceptible to retinal ganglion cell loss in age, glaucoma, and traumatic optic neuropathy. Spp1 deficiency impairs mitochondrial function and phagocytosis and increases expression of inflammatory markers, whereas Spp1 overexpression strongly increases ganglion cell survival and protects visual function.

Graphical Abstract

*Correspondence: song_li@meei.harvard.edu (S.L.), tatjana_jakobs@meei.harvard.edu (T.C.J.).

AUTHOR CONTRIBUTIONS

S.L. and T.C.J. devised the experiments and wrote the paper. S.L. performed all experiments on astrocyte and ganglion cell cultures, and T.C.J. performed the electron microscopic imaging. S.L. and T.C.J. performed *in vivo* studies on mice, immunohistochemistry, and qPCR. S.L. and T.C.J. analyzed the data. S.L. wrote the R scripts for RNA sequencing analyses.

DECLARATION OF INTERESTS

The authors declare no competing interests.

SUPPLEMENTAL INFORMATION

Supplemental information can be found online at https://doi.org/10.1016/j.celrep.2022.111880.

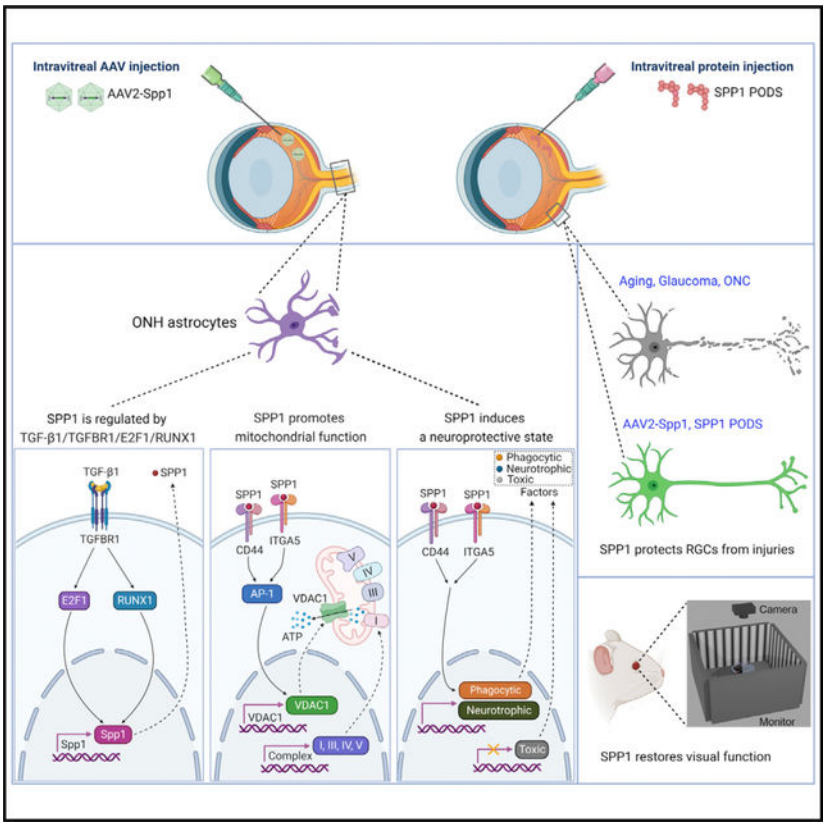

INTRODUCTION

Aging in the CNS progressively leads to tissue dysfunction and loss of neurons. In the retina, this manifests as loss of photoreceptors and retinal ganglion cells (RGCs), the only projection neuron of the retina whose axons form the optic nerve (ON). Mammalian retinas lose RGCs even during normal aging.[1] In mice, the loss rate is about 7,000 cells per year from about 50,000 in early adulthood.[2] Superimposed on this “normal” decline in visual function are degenerative diseases of the retina that expedite the rate of neuron degeneration, with age-related macular degeneration and glaucoma being clinically most relevant.[3,4] Therapeutic approaches to these diseases are complicated because their pathophysiology resembles normal aging in many ways.[5] On the other hand, a better understanding of age-related changes may also lead to development of therapies against neurodegenerative diseases such as glaucoma.

We focus on glaucoma firstly because it is one of the leading causes of blindness in industrialized countries and secondly because RGCs may be a more generalizable model of neurodegeneration than the highly specialized photoreceptors. Glaucoma is characterized by progressive apoptotic loss of RGCs and degeneration of the optic nerve.[6] Elevated intraocular pressure (IOP), genetic factors, and age are the most important risk factors. Lowering the IOP is currently the mainstay of glaucoma management, but additional neuroprotective approaches would be welcome.

Recently, several approaches to an anti-aging therapy have been proposed, and proof-of-principle experiments in the visual system suggest that rescuing ganglion cells is possible. A recent study used virus-mediated overexpression of three of the Yamanaka factors in RGCs to protect RGCs from glaucoma and age-related cell loss, mediated by restoration of a “youthful” epigenetic profile in experimental mice.[7] Another change associated with aging is a gradual increase in sterile inflammation, which is likely triggered when age-related decline in autophagy leads to gradual accumulation of cellular debris, chronic activation of the inflammasome, and production of pro-inflammatory cytokines.[8] Finally, a decline in mitochondrial function, decreased ATP production, excessive generation of radical oxygen species, and failure of mitochondrial quality control have been implicated in age-related neurodegenerative diseases. On the other hand, interventions that stimulate mitochondrial function, such as aerobic exercise, are protective.[9,10]

Age-related changes are observed not only in neurons but also in glial cells.[11–13] RNA sequencing of purified astrocytes from various regions of the brain has demonstrated up-regulation of inflammatory markers, components of the complement cascade, factors involved in synapse elimination, and others that are similar to those observed in reactive astrocytes.[14–16] In the optic nerve head, astrocytes form the direct cellular environment of the unmyelinated RGC axons.[17,18] One of their physiological functions is to phagocytose axonal mitochondria that have reached the end of their life cycle in a process referred to as transmitophagy.[19] An age-related decrease in the phagocytic capacity of astrocytes may contribute to accumulation of damaged mitochondria in RGCs themselves.

Using a new reporter/conditional knockout strain of mice, we report that loss of SPP1 leads to a premature aging phenotype in the visual system of mice that is characterized by up-regulation of inflammatory markers, decreased mitochondrial and phagocytic function of astrocytes, increased vulnerability to glaucomatous RGC loss, and an accelerated age-related decline in vision. Overexpression of SPP1 in the retina and optic nerve head of normal C57BL/6 mice apparently slows aging in the visual system, protects RGCs, and restores vision in several models of optic nerve damage.

RESULTS

Deletion of Spp1 leads to accelerated ganglion cell loss and vision decline in aging, glaucomatous, and axotomized retinas

Interfering with astrocyte reactivity in mouse models of glaucoma leads to a worse outcome for visual function and RGC survival,[20] indicating that reactive astrocytes play a protective role, at least in the early stages of the disease. In search of astrocyte-derived factors that may be used therapeutically, we surveyed gene expression studies of reactive astrocytes in various disease models (experimental glaucoma, optic nerve crush (ONC), middle cerebral artery occlusion, and lipopolysaccharide (LPS)–induced neuroinflammation) and used *in silico* analysis to find genes and pathways that were differentially regulated in reactive astrocytes.[21–26] We chose SPP1 as a candidate molecule because it was up-regulated in most datasets and participated in a network containing transforming growth factor β1 (TGF-β1) and at least the transcription factors RUNX1 and E2F1, which regulate SPP1 expression and are also up-regulated in glaucoma and optic nerve injury.[27–29]

We used mice with global deletion of the Spp1 gene (Spp1 knockout [KO]) to test whether the RGCs in this strain are more susceptible to damage because of age, elevated IOP, and optic nerve crush. We first examined the retinas of Spp1 KO animals for abnormalities that may confound our analysis (Figure S1A). There were no differences between young (3-month-old) Spp1 KO mice and C57BL/6 mice observed in optical coherence tomography, immunostaining for several cell type markers (Figures S1B–S1J), or electron microscopy of the retinas (Figures S1K and S1L).

During aging, Spp1 KO mice lost RGCs faster than wild-type C57BL/6 mice (Figures 1A and 1B), which agrees with an earlier study.[30] To test the function of SPP1 in glaucoma, we used the microbead occlusion model in 3-month-old mice[31] to induce unilateral elevated IOP and analyzed RGC survival, visual acuity, and the pattern electroretinography (ERG) amplitude (Figure S2A). Spp1 KO and wild-type retinas at that age started with similar numbers of ganglion cells, and 1 month after microbead injection, wild-type C57BL/6 mice lost 32% of the $BRN3A^+$ RGCs in the experimental eye, which was expected in this model. Spp1 KO mice had a similar increase in IOP (IOP curves over time are shown in Figure S2B), but the loss of $BRN3A^+$ ganglion cell numbers was significantly worse, about 48% (Figures 1C and 1D). The increased RGC degeneration was reflected in visual function, which was also significantly more severely affected in the Spp1 KO animals (Figures 1E, 1F, S2C, and S2D). Although BRN3A is a common marker of RGCs in healthy and glaucomatous retinas,[32,33] there is the possibility that it is down-regulated in disease[34] and that lack of BRN3A staining indicates dysfunctional cells rather than complete disappearance of the cells after apoptosis.[35,36] Therefore, we counted ganglion cell axons in the optic nerve after paraphenylenediamine (PPD) staining. As expected for young animals, there was no difference at baseline between wild-type C57BL/6 and Spp1 KO mice, and both groups lost axons after induction of elevated IOP (Figure 1G). There was a significant difference between wild-type and the Spp1 KO mice, which lost more axons (Figures 1G and S2E). Finally, we calculated the cumulative IOP insult, defined as the area under the curve of IOP versus time, showing that both groups had received a similar injury (Figure 1H). These data indicate that RGCs in Spp1 KO animals react more sensitively to glaucomatous injury than their wild-type counterparts.

After optic nerve crush, ganglion cells degenerate and die in a time-dependent manner.[37] Pattern ERG and optomotor reflex cannot be elicited in the affected eye after an optic nerve crush lesion and were therefore not tested. In Spp1 KO mice, ganglion cell loss was accelerated compared with wild-type mice, but the severe nature of the optic nerve crush injury eventually led to almost complete loss of ganglion cells in both strains (Figures 1I and 1J).

Regulation of SPP1 expression in reactive astrocytes by a signaling cascade consisting of TGF-β1/TGFBR1/RUNX1/E2F1

In the uninjured optic nerve, SPP1 was detectable only in axons of intrinsically $SPP1^+$ alpha ganglion cells[38] and absent from glial cells (Figure 2A). After elevation of IOP, and especially after optic nerve crush injury, SPP1 was strongly up-regulated (Figure 2A). Counterstaining with the astrocyte marker glial fibrillary acidic protein (GFAP) showed

that most SPP1^{+} glial cells were astrocytes, but some cells with microglial morphology were also observed (Figure 2B). To identify signaling pathways that were responsible for up-regulation of SPP1 in reactive astrocytes, we used cell cultures of GFAP^{+} astrocytes from newborn mice (Figure S3A). After 14 days in culture, we detected RUNX1, E2F1, and SPP1 expression and co-localization of SPP1 with RUNX1 and E2F1 (Figures 2C and S3A). The astrocytes started expressing SPP1, most likely because of the tendency of astrocytes to assume a reactive phenotype in culture.[39] We took advantage of this behavior to verify that Spp1 is regulated by TGF-β1, RUNX1, and E2F1 in astrocytes. Expression of Spp1, E2f1, and, to a lesser extent, Runx1 was induced by treatment of cultured astrocytes with recombinant TGF-β1, and the effect was completely abolished by the TGF-β1 receptor blocker SB431542 (Figures 2D and S3B–S3E). Inhibition of RUNX1 with Ro5-3335 and E2F1 with HLM006474 alone decreased SPP1 immunolabeling and Spp1 mRNA expression and blocked the TGF-β1-induced increase in SPP1 expression in astrocytes (Figures 2E–2G, S3F, and S3G).

To assess the gene expression pattern *in vivo*, we crossed B6.GFAP-cre, a strain expressing cre recombinase under control of the astrocyte-specific GFAP promoter, with a tdTomato reporter strain (Ai14) and collected tdTomato-labeled astrocytes by fluorescence-activated cell sorting (FACS). Tgf-β1, Runx1, E2f1, and Spp1 were up-regulated in astrocytes *in vivo* after elevation of IOP and optic nerve crush compared with naive control nerves (Figure S4A).

Conditional deletion of Spp1 in astrocytes

Analysis of SPP1 activity *in vivo* is complicated by the fact that SPP1 is expressed not only in reactive astrocytes but also physiologically in alpha ganglion cells and microglia. To dissect the mechanisms of SPP1-mediated neuroprotection in more detail, we designed a new strain suitable for conditional deletion of Spp1 with *loxP* sites flanking exons 4–7 of the Spp1 gene (Spp1$^{GFPfl/fl}$). Before recombination, the mice expressed Spp1, followed by P2A-EGFP from the endogenous Spp1 locus. By crossing with a strain that expresses cre under control of the Gfap promoter, the Spp1/EGFP cassette was eliminated, and tdTomato was expressed (Spp1$^{GFPfl/fl}$GfapCre; Figure 3A). We first verified that tdTomato fluorescence was detectable in optic nerve astrocytes and that no EGFP was co-localized with tdTomato in Spp1$^{GFPfl/fl}$GfapCre mice at baseline (Figure 3B). No SPP1 immunoreactivity was detectable in optic nerve astrocytes from Spp1$^{GFPfl/fl}$GfapCre mice (Figure S4B). In FACS-sorted astrocytes from Spp1$^{GFPfl/fl}$GfapCre mice, no expression of Spp1 mRNA was detected, confirming conditional deletion of Spp1 in astrocytes (Figure S4C).

We repeated the aging, IOP elevation, and optic nerve crush experiments in Spp1$^{GFPfl/fl}$GfapCre mice to determine whether it was specifically the loss of astrocytic SPP1 that was responsible for the increased RGC vulnerability. Spp1$^{GFPfl/fl}$ mice were used as controls, and they lost about 32% of their RGCs over a period of 16 months, the expected rate in mice on the B6 background, but cell loss in Spp1 conditional knock-out (cKO) strain Spp1$^{GFPfl/fl}$GfapCre mice was significantly worse over the same time period (44% in Spp1 cKO versus 32% in control; Figures 3C–3E). Similarly, after induction of elevated IOP, Spp1

cKO mice did worse in terms of ganglion cell survival and visual function (Figures S4D and 3F–3I). We also followed the timeline of RGC loss after optic nerve crush in the cKO and the control strain. Similar to global Spp1 KO, astrocytic Spp1 cKO led to faster cell loss after optic nerve crush (Figures 3J and 3K).

Astrocytes are the major glial component of the unmyelinated optic nerve head (ONH), but microglial cells are also present in the nerve and the retina, and Müller glia are abundant in the retina. In some injuries, Müller glia are known to up-regulate GFAP; thus, Gfap-driven cre may be active in Müller cells. We stained vertical sections of retinas for SPP1 and the Müller cell marker glutamine synthetase (GS) and found no SPP1 immunoreactivity in Müller cells, in uninjured young retinas, or after optic nerve crush or an elevation of IOP, or in aging (Figure 3L). Microglia were negative for SPP1 expression in naive nerves, but they did transiently become $SPP1^{+}$ after nerve injury. This can be seen in Figure 3B, where the green cell bodies are microglia that expressed EGFP in Spp1 cKO animals. As expected, Gfap-cre did not lead to Spp1 deletion in microglia. The experiments in conditional Spp1 KO animals demonstrated that it is specifically astrocytic Spp1 production that is responsible for the neuroprotective effects of this factor.

Spp1 deletion induces neurotoxic astrocytes *in vitro* and *in vivo*

To understand the molecular mechanism of SPP1 activity in astrocytes, we carried out RNA sequencing from cultured Spp1 KO astrocytes versus wild-type C57BL/6 controls (Figure S5A; GEO: GSE174522; volcano plot and pathway analysis are shown in Figures S5B and S5C). Pathway analysis of the differentially expressed genes (defined as at least 1.5-fold up- or down-regulation and adjusted $p < 0.05$) revealed that two major pathways were differentially regulated in Spp1 KO astrocytes; oxidative phosphorylation was predicted to be inhibited, and neuroinflammatory markers were up-regulated (Figures 4A and S5C).

A recent publication reported three sets of marker genes that were expressed in reactive astrocytes: a “pan-reactive” set commonly expressed in reactive astrocytes, an “A1” (or neuroinflammatory) set associated with some pathological conditions (such as LPS injection), and an “A2” (or neuroprotective) set associated with other conditions, such as cerebral artery occlusion.[40] In Spp1 KO astrocytes, most pan-reactivity markers were up-regulated, as were most “A1” markers. Almost all markers specific for the “A2” neuroprotective type were down-regulated (Figures 4B and S5D), indicating that Spp1 deletion induced “A1” astrocytes. Inhibition of TGFBR1 with SB431542 and RUNX1 with Ro5-3335 induced a neurotoxic A1-like pattern (Figures S5E and S5F). Inhibition of E2F1 with HLM006474 did not specifically induce the A1- or A2 astrocyte phenotype but caused down-regulation of most genes in all groups (Figure S5G). Complement component C3, which was virtually undetectable in wild-type optic nerve astrocytes, was strongly up-regulated in Spp1 KO cells (Figures 4C–4E and S6A–S6C). We also found that genes associated with synaptogenic and neurotrophic activity were down-regulated in Spp1 KO astrocytes (Figures 4F and S6A).

Astrocytes are known to be phagocytic *in vitro* and *in vivo*.[19,41] In our dataset, several phagocytosis-related genes were differentially regulated, most notably Megf10, which has been reported as a C1q receptor involved in phagocytic activity of astrocytes.[42] On the other

hand, there was no clear trend for the TAM receptors Tyro3, Axl, and Mertk, with Mertk and the ligand Gas6 up-regulated and Axl and Tyro3 down-regulated in the Spp1 KO astrocytes (Figure 4F). To rule out a general deficiency in motility of Spp1 KO astrocytes, we tested migration in a scratch assay (Figure S6D). Spp1 KO astrocytes filled the gap faster than wild-type astrocytes, but this may be primarily due to the increased cell proliferation of the KO cells. A bromodeoxyuridine (BrdU) incorporation assay showed that 10% of Spp1 KO astrocytes incorporated the BrdU label versus 5% of wild-type cells (Figures S6E–S6G).

Because these experiments relied on cultured astrocytes, we verified the results with an analysis of freshly isolated optic nerve head $SPP1^{+}$ astrocytes from Gfap-tdTomato and $SPP1^{-}$ astrocytes from $Spp1^{GFPfl/fl}$GfapCre (cKO) mice (Figures 4G and S7A–S7C). The expression profiles of $Spp1^{+}$ and Spp1 KO astrocytes were compared in naive nerves with no injury and nerves after elevation of IOP or optic nerve crush injury. Most synaptogenic, phagocytic, and neurotrophic markers were down-regulated in Spp1 cKO astrocytes compared with wild-type ones. In contrast, C3 and (in the high-IOP condition) C1q expression in cKO astrocytes exceeded that of the wild type (Figures 4H and S7D).

We also tested the expression pattern of A1- and A2-specific genes in response to elevation of IOP and optic nerve crush *in vivo* (Figure S8A). Without injury, Spp1 KO astrocytes showed an “A1” type with up-regulation of A1-specific genes and down-regulation of most A2-specific genes compared with wild-type nerves (Figure S8B). However, after IOP elevation or crush injury, there was no clear pattern indicative of an “A1” or “A2” type in $Spp1^{+}$ astrocytes or Spp1 KO astrocytes *in vivo* (Figures S8C–S8H). These data show that Spp1 deletion induces a neurotoxic phenotype in astrocytes *in vitro* and *in vivo*, mainly including activation of neuroinflammation and neurotoxic factors and inhibition of synaptogenic, phagocytic, and neurotrophic processes.

Spp1 depletion leads to impaired phagocytosis in astrocytes

Because several phagocytosis-related genes were differentially regulated in Spp1 KO astrocytes, we tested the overall functional effect on astrocyte phagocytosis in a pHrodo incorporation assay and found that the percentage of cells with incorporated pHrodo was the same, but the amount of the incorporated label was lower in Spp1 KO astrocytes than that in wild-type astrocytes, indicating impaired phagocytosis (Figures 4I–4K). Similarly, we also found decreased phagocytic activity in Spp1 KO astrocytes by an assay based on relative fluorescence intensity of pHrodo particles in astrocytes (Figure 4L).

Astrocytes have been implicated in degradation of axonal mitochondria, a process that involves phagocytosis of axonal evulsions that contain damaged mitochondria by neighboring astrocytes.[19] This process relies at least in part on LGALS3 (Galectin 3).[41] Lgals3 mRNA is detectable at similar levels in uninjured nerves from wild-type and Spp1 KO mice, and it is up-regulated by an increase in IOP and optic nerve crush injury in optic nerves of wild-type animals, only to a very limited extent in the KO (Figure 4M), suggesting that Spp1 deficiency prevented the injury-induced increase in Lgals3 expression. In cultured astrocytes, rSPP1 protein directly up-regulated Lgals3 gene expression almost 2-fold (Figure 4N). *In vivo*, LGALS3 immunoreactivity was detectable in the ONH and ON of naive C57BL/6 and Spp1 KO mice, but injury-induced up-regulation of LGALS3 was

markedly reduced in the Spp1 KO (Figure 4O). LGALS3 expression was lower in old (16 month) C57BL/6 mice, suggesting lower phagocytic activity of aged astrocytes (Figure 4O).

Spp1 deletion causes mitochondrial dysfunction

Because oxidative phosphorylation was one of the major down-regulated pathways in Spp1 KO astrocytes (Figure 5A) that affected genes complexes I, III, IV, and V of the electron transport chain (Figures S9A and S9B), we used metabolic analysis to measure mitochondrial respiration in Spp1 KO versus wild-type astrocytes. Oxygen consumption rate (OCR) and extracellular acidification rate (ECAR) (Figures 5B and 5C), basal and maximal respiration, and ATP production were significantly lower in Spp1 KO astrocytes (Figures 5D–5F), indicating impaired mitochondrial respiration in Spp1 KO astrocytes. We tested whether genes related to oxidative phosphorylation are also down-regulated in Spp1 KO astrocytes *in vivo*. Making use of red fluorescent protein expression in cKO animals, we used FACS to isolate Spp1^{-} astrocytes. Cells from Gfap-tdTomato served as controls. Although cKO optic nerves did not contain fewer cells, the yield of Spp1^{-} cells was consistently lower than that of wild-type astrocytes, suggesting that Spp1^{-} cells do not withstand the dissociation procedure as well as their wild-type counterparts. As in cell culture, we found marked down-regulation of several genes related to oxidative phosphorylation (Figure 5G).

TGF-β1 positively regulated SPP1, and TGF-β1 induced increased OCR, ECAR, basal and maximal respiration, and ATP production in cultured astrocytes, an effect that was blocked by the TGF-β1 receptor blocker SB431542 (Figures S9C–S9G), the RUNX1 antagonist Ro5-3335 (Figures S9H–S9L), and the E2F1 antagonist HLM006474 (Figures S9M–S9Q). In electron microscopy of the unmyelinated portion of the optic nerve, Spp1 KO mice showed a high prevalence of axonal mitochondria with few or no cristae even at young ages (Figure 5H). Degenerating mitochondria were also present in the astrocytes, especially in aged animals (Figures 5I and 5J).

Exogenous recombinant SPP1 restores astrocytic gene expression

Recombinant SPP1 (rSPP1) protein significantly inhibited expression of C3 in cultured C57BL/6 astrocytes (Figure S10A). Exogenous rSPP1 was also found to stimulate expression of the astrocytes' own Spp1 gene, an effect that was dependent on the SPP1 receptor Itgα5 but not on the other known SPP1 receptor, CD44 (Figure S10B). We also found that rSPP1 reversed the decreased expression of "A2" genes to almost normal levels but had little effect on expression of "A1" genes in Spp1 KO astrocytes (Figure S10C). Recombinant SPP1 also restored expression of phagocytosis-related genes, neurotrophic factors, and genes related to oxidative phosphorylation and inhibited toxic factor C1q and C3 expression in Spp1 KO astrocytes (Figures S10D and S10E). There was no further effect of rSPP1 on expression of oxidative phosphorylation-related genes in wild-type astrocytes (Figure S10F).

SPP1 UP-REGULATES VDAC1

The Vdac1 (voltage-dependent anion channel 1) gene was significantly down-regulated in Spp1 KO astrocytes in our RNA sequencing dataset, by qPCR, and in

immunohistochemistry (Figures 5A, S9B, and 6A–6C). SPP1 and VDAC1 were co-expressed in cultured astrocytes (Figure S11A). Recombinant SPP1 led to a significant increase in VDAC1 labeling intensity in cultured wild-type astrocytes and to a 50-fold increase in Vdac1 mRNA expression. This effect was inhibited by knockdown of the SPP1 receptors CD44 and Itgα5 and by inhibition of AP1, which is downstream in the SPP1 signaling pathway[43] (Figures 6D–6F; qPCR validation for the small interfering RNAs [siRNAs] is shown in Figures S11B–S11D). TGF-β1 increased expression of Vdac1 mRNA, and the effect was prevented by RUNX1 and E2F1 inhibition (Figure 6G). Recombinant SPP1 increased OCR, ECAR, basic respiration, maximal respiration, and ATP production in astrocytes in a dose-dependent manner (Figures 6H–6L). This effect was abolished by treating the astrocytes with Vdac1 siRNA or metformin, an inhibitor of VDAC1 activity (Figures 6M–6Q).

SPP1 increases intracellular ATP concentration via VDAC1

Because VDAC1 allows diffusion of ATP from mitochondria into the cytoplasm, we wanted to determine whether SPP1 administration leads to an increase in cytosolic ATP concentration via VDAC1. We visualized cytosolic ATP in astrocytes by transfection with a plasmid encoding the ATP sensor iATPsnFR and an mCherry tag.[44] The ATP sensor increased in fluorescence upon binding ATP (Figure 6R). Exogenous rSPP1 led to an increase in cytosolic fluorescence, indicating that SPP1 not only increased mitochondrial ATP production but also promoted its delivery into the cytosol. Increased fluorescence of the ATP sensor induced by rSPP1 was blocked by Vdac1 knockdown, suggesting that SPP1 promoted ATP delivery into the cytosol through up-regulation of VDAC1 (Figures 6R and 6S).

Astrocytic SPP1 enhances neurite growth and branching in RGCs in a VDAC1-dependent manner

We used co-culture of wild-type RGCs and astrocytes from wild-type or Spp1 KO mice to test how they affect the growth of ganglion cells. Wild-type astrocytes supported the growth of RGCs with complex branching patterns (Figure S11E). When ganglion cells were grown on Spp1 KO astrocytes, they had fewer processes overall and fewer higher-order branches (Figures 6T and S11F). This was quantified by Scholl analysis (Figure 6U) and measurement of total process length (Figure 6V). We co-cultured wild-type ganglion cells on wild-type astrocytes that were pre-treated with Vdac1 siRNA or the VDAC1 inhibitor metformin for 24 h and washed extensively with medium before seeding the ganglion cells. Because of the time limitations of siRNA or metformin activity, RGC neurite length was measured 1 and 2 days after seeding. On day 1, the ganglion cells growing on astrocytes with VDAC1 inhibition already showed significantly decreased total neurite growth and slightly reduced branching (Figures S11G and S11H). On day 2, total process length and number of higher-order branches were increased in the vehicle group compared with day 1. However, total process length and number of higher-order branches were decreased after VDAC1 inhibition by Vdac1 siRNA or treatment with the inhibitor metformin in a manner very similar to that of Spp1 KO astrocytes (Figures 6W and 6X). These results suggest that SPP1 promotes RGC neurite growth and branching via VDAC1.

SPP1 acts as an anti-aging factor in the visual system

We next tested whether adeno-associated virus type 2 (AAV2)-mediated overexpression of SPP1 would have an anti-aging effect. AAV2 is not specific to astrocytes, but we reasoned that, as a secretory protein, SPP1 from any source may be beneficial. We injected young (4-month-old) C57BL/6 mice intravitreally with AAV2-Spp1-EGFP (hereafter called AAV2-Spp1). Age-, strain-, and sex-matched control animals received AAV2-EGFP. One year later, the pattern ERG and visual acuity of the mice were measured, and RGCs were counted (Figure 7A). As expected, the control animals showed loss of RGCs in the retina, a decrease in pattern ERG amplitude, and a moderate reduction in visual acuity. In aged animals treated with the AAV2-Spp1 construct, RGC counts and visual function were significantly better than in the controls (Figures 7B–7D).

In electron microscopy, a characteristic feature of aging is increasing numbers of enlarged axons with pale axoplasm and swollen mitochondria with reduced cristae.[2] These changes progress in a predictable manner so that it is possible to determine the age of an animal from the variance of axon diameters in the optic nerve head.[2] We imaged the unmyelinated segments of optic nerves from AAV2-Spp1-treated and AAV2-EGFP-treated animals and measured axon diameters (Figures 7E and 7F). Nerves treated with control virus AAV2-EGFP showed enlarged axons and damaged mitochondria. These features were not found in AAV2-Spp1-treated aged nerves, suggesting that SPP1 overexpression slows the effects of normal aging and preserves vision in aging mice.

SPP1 overexpression rescues RGCs and visual function

Young C57BL/6 mice were injected with AAV2-Spp1 or AAV2-EGFP, expression of the constructs was verified by fundus photography 1 month after injection, and the IOP was elevated using the microbead injection method (Figures S12A–S12G, S13, and S14 show transfection efficiencies and co-expression of SPP1 and EGFP from the AAV2-Spp1 construct in cells that were not intrinsically $Spp1^{+}$). Treatment with AAV2-Spp1 had a strong protective effect on RGC counts, pattern ERG amplitude, and visual acuity (Figures 7G–7J). This effect was more pronounced in glaucomatous wild-type retinas, where SPP1 overexpression restored visual function and RGC numbers almost to baseline levels, but it was also observed in Spp1 KO animals. However, in Spp1 KO animals, visual function did not completely recover, possibly indicating that the SPP1 expression levels in the optic nerve were not sufficient because AAV2 did not penetrate deeply into the nerve. Treatment with AAV2-Spp1 also led to preservation of about 38% of RGCs 2 weeks after an optic nerve crush injury, whereas, under the control condition, all but 4% of the RGCs had degenerated by this time (Figures 7G and 7H).

Last, we elevated the SPP1 levels in the retina by intravitreal injection of SPP1-polyhedrin complexes (Polyhedrin Delivery System, SPP1 PODS) that act as a slow-release depot of SPP1 protein. SPP1 PODS were effective in preserving visual function and RGC numbers in mouse models of glaucoma and optic nerve crush, but not to the same level as the AAV2-Spp1 construct (Figures 7K–7N). Isolated astrocytes from optic nerves treated with SPP1 PODS showed increased expression of most genes related to mitochondrial function in our set, increased phagocytic and neurotropic markers, and slightly reduced expression

of C3 and Tnf (Figure 7O). Our data suggest that overexpression of SPP1 is an effective approach to counteract the effects of aging on the visual system and to treat a major, age-related disease.

DISCUSSION

Here we demonstrate that SPP1 is significantly up-regulated in optic nerve astrocytes after injury. This effect is mediated by the transcription factors RUNX1 and E2F1, with TGF-β1 as an upstream regulatory factor. SPP1 stimulates mitochondrial activity and ATP production, secretion of neurotropic factors, and phagocytosis. Expression of neurotoxic and inflammatory mediators is negatively regulated by SPP1. These findings suggest a neuroprotective role of SPP1 that may be used therapeutically in conditions such as glaucoma. Our study shows that virus-mediated overexpression or direct injection of the protein is highly protective of RGCs in several models of RGC degeneration.

In normal retinas, SPP1 immunoreactivity is restricted to alpha RGCs.[38,45] We did not observe SPP1 in other neurons or in Müller glia in uninjured retinas at any age or after optic nerve damage. Optic nerve astrocytes, however, strongly up-regulated SPP1 after an increase in IOP or an optic nerve crush injury. Similar up-regulation was found in brain astrocytes after ischemia,[25] suggesting that SPP1 is a common marker of reactive astrocytes. This does not necessarily indicate a neuroprotective role of SPP1 because astrocytes react to injury with a program of morphological, metabolic, and transcriptomic changes, not all of which are beneficial.[46] In some injury models, it is possible to distinguish harmful ("A1") and neuroprotective ("A2") phenotypes of reactive astrocytes by arrays of 12 marker genes each that are typically expressed. The "A1" type of reactivity is induced by microglia-derived IL-1α, TNF, and C1q upon LPS-induced neuroinflammation.[40] Other conditions, such as ischemia[25] or optic nerve crush,[26] induce a phenotype that would be characterized as neuroprotective ("A2") by these criteria. However, as useful as such transcriptomic characterizations are, they should not be interpreted as defining fixed cell types.[47] In many cases, expression profiles of "A1" and "A2" genes overlap in the same population of reactive astrocytes, there is considerable heterogeneity between astrocytes even in the same anatomical region, and astrocyte reactivity itself can be reversible when the pathological stimulus is removed.[48–51] In aging, astrocytes take on a more neurotoxic phenotype,[15,52] are less phagocytic, and show declining mitochondrial function.[53]

Our data indicate that supplying a single protein, SPP1, slows the course of age-related or glaucomatous death of RGCs and the concomitant loss of visual function. It does so by mitigating several facets of the decline in astrocyte function. First, "A2" markers are down-regulated in Spp1 KO astrocytes, suggesting that they have a more neurotoxic profile. Consistent with this observation, neuroinflammatory markers are up-regulated in Spp1 KO astrocytes. Neuroinflammation is observed in human glaucomatous optic nerves and retinas,[54] and it is a common feature of animal models of the disease.[55–57] Aging, a major risk factor for glaucoma, leads to chronic low-grade inflammation of the CNS.[58] In Spp1 KO astrocytes, production of inflammatory mediators is chronically elevated, even at a young age, whereas the neurotrophic factors are down-regulated. This may shift the balance

of protective and detrimental functions into the neurodegenerative direction and expedite natural age-related ganglion cell loss and increase susceptibility to glaucoma.

Our data also indicate that, in young Spp1 KO mice, the mitochondria of RGCs show morphological abnormalities, such as lack of cristae, that are usually a feature of advanced age.[2] On the molecular level, Spp1 deficiency causes decreased expression of genes involved in oxidative phosphorylation. Functionally, Spp1 deletion leads to a decrease in oxidative phosphorylation and ATP production. Because phagocytosis is a highly energy-dependent process,[59] decreased mitochondrial function may partly explain the marked reduction of phagocytic activity we observed in Spp1 KO astrocytes. In the optic nerve, impaired mitochondrial function and reduced phagocytosis may simultaneously negatively affect axonal integrity from two sides. Astrocytes, especially those of the myelination transition zone, are phagocytic[41] and play an active role in degradation of axonal mitochondria that have reached the end of their life cycle. In transcellular mitophagy, spent axonal mitochondria are accumulated in bag-like evulsions from the axonal membrane that are engulfed and phagocytosed by surrounding astrocytes.[19,60] This process is not pathological because it is observed even in naive young optic nerves,[2] and in neurons with long axons, transcellular mitophagy may be an energy-saving mechanism that obviates the need to transport mitochondria all the way back to the cell's soma for degradation.[60] Accumulation of abnormal axonal mitochondria in the axons of Spp1 KO mice may therefore be due to a combination of impaired mitochondrial function and impaired phagocytosis.

Astrocyte-specific deletion of Spp1 leads to an increase in RGC vulnerability to injury, but astrocytes are not the only potential source of SPP1 in the visual system. Alpha RGCs, but not other types of RGCs, intrinsically express SPP1 and are more resistant to optic nerve damage than most other types of RGCs.[38,61] The physiological function of SPP1 in these cells is not known. Possibly, alpha cells secrete SPP1 in response to injury and take part in the retina's defense against neurodegeneration in conditions like glaucoma or traumatic injury, but this remains to be proven. Microglia briefly express SPP1 (or EGFP in $Spp1^{fl/fl}$GfapCre mice) after optic nerve crush. Spp1 mRNA expression has also been detected in activated retinal microglia.[62,63] All of these cells could secrete SPP1 in response to injury.

Whether Müller cells are a source of SPP1 *in vivo* is less clear. SPP1 is expressed in cultured Müller cells,[64] particularly upon glial cell line-derived neurotrophic factor (GDNF) stimulation,[65] and SPP1 has been found in activated Müller cells from surgical specimens of epiretinal membranes,[66] but Spp1 KO does not affect Müller cell structure.[30] In our study, we did not observe SPP1 expression in Müller cells in uninjured young retinas or after optic nerve crush or an elevation of IOP, or in aging. However, because SPP1 is a secreted protein, from a therapeutic point of view, the source may not matter. AAV2 does not specifically target astrocytes, and we were able to elicit a neuroprotective effect even with the protein itself. However, although AAV-mediated overexpression of Spp1 preserved RGC function not only in wild-type C57BL/6 retinas but also in Spp1 KO retinas, it did not do so to quite the same extent. This may be due to the difficulty of transfecting astrocytes located deep in the optic nerve, but there is the possibility that endogenous SPP1 (e.g., coming from microglia or alpha RGCs) is also needed for the full neuroprotective effect.

Our data suggest that SPP1 may have potential as a neuroprotective treatment that could be combined with IOP-lowering drugs that currently are the first-line treatment of glaucoma.[67] As a protein, SPP1 would have to be injected into the vitreous. Intraocular injection is commonly used in anti-VEGF (vascular endothelial growth factor) therapy for age-related macular degeneration, but it requires repeated injections over a long period of time. An alternative strategy might be to use upstream regulators to induce SPP1 expression. TGF-β1 or RUNX1 activation would likely not be viable approaches because of the pro-fibrotic effects in the anterior chamber in the case of TGF-β1[68] and the potential for stimulation of aberrant blood vessel formation in the case of RUNX1.[69] Currently, AAV-mediated overexpression of Spp1 might be the best option. AAV is generally considered safe,[70–72] and several clinical trials for monogenic eye diseases in humans are under way or have been completed.[73–76] SPP1 may be a candidate for AAV-mediated gene therapy if safety and long-term efficacy can be established.

Limitations of the study

Using SPP1 therapeutically in glaucoma or other neurodegenerative diseases requires SPP1 overexpression to be free of negative side effects in the long term. We did not observe detrimental effects of SPP1 on any structure in the murine eye, even in our long-term overexpression experiment. However, the maximum life expectancy of mice is about 36 months, and a glaucoma therapy would most likely span decades. The effect of SPP1 overexpression needs also to be studied in a long-lived species, preferably a non-human primate.

Another limitation of the present study stems from the fact that SPP1 expression is not restricted to reactive astrocytes. Alpha RGCs and microglia may be additional sources of SPP1. An analysis of conditional Spp1 KO, especially in microglia or alpha RGCs, would be of interest.

STAR★METHODS

RESOURCE AVAILABILITY

Lead contact—Lead contact is Tatjana C. Jakobs (tatjana_jakobs@meei.harvard.edu).

Materials availability—Further information and requests for resources and reagents in this study are available upon reasonable request to lead contact with a completed Materials Transfer Agreement.

Data and code availability

- RNA-sequencing data have been deposited at NCBI Gene Expression Omnibus (GEO) and are publicly available as of the date of publication. Accession numbers are listed in the key resources table. High resolution TEM microphotographs have been deposited at the Harvard Dataverse (dataverse.harvard.edu). The DOI is listed in the key resources table.
- All original code has been deposited at GitHub and is publicly available as of the date of publication. DOIs are listed in the key resources table.

- Any additional information required to reanalyze the data reported in this paper is available from the lead contact upon request.

EXPERIMENTAL MODEL AND SUBJECT DETAILS

Animals—Spp1 KO (B6.129S6(Cg)-Spp1^{tm1Blh}/J) mice were obtained from the Jackson Laboratories (stock number 004936) and maintained in our facility as homozygous breeding stock. This strain is deficient for SPP1 expression in all tissues. C57BL/6 mice (Jackson Laboratories, stock number 000664) were used as controls. The strain, B6.Spp1$^{fl\text{-}EGFP\text{-}stop\text{-}tdTomato}$, for conditional deletion of Spp1 was produced by Cyagen. The cre donor strain for creating the astrocyte specific deletion was B6.Cg-Tg(Gfap-cre) 77.6Mvs/2J (Jackson Laboratory, stock number 024098). The reporter strain Ai14 to create Spp1^{+} astrocytes expressing red fluorescent protein was B6.Cg-Gt(ROSA)26Sor$^{tm14(CAG\text{-}tdTomato)Hze}$/J (Jackson Laboratory, stock number 007914). Male and female mice were used in equal numbers, and all control mice were strictly age- and sex- matched. Experiments included young adult mice (3–5 months) and aged mice (16 months). Mice were kept at a 12 hour dark/light cycle and received water and standard food at libitum. Mice were anesthetized by i.p. injection of ketamine/xylazine (100 mg/kg and 10 mg/kg, respectively), supplemented by topical application of 0.5% proparacaine to the ocular surface. After surgery, mice received an s.c. injection of 0.1 mg/kg buprenorphine. At the end of the experimental period, mice were euthanized by CO_2 inhalation according to the Guide for the Care and Use of Laboratory Animals of the AAALAC. All animal procedures were done in accordance with the guidelines of the Association for Research in Vision and Ophthalmology and approved by the Institutional Animal Care and Use Committee at Schepens Eye Research Institute.

Primary cell culture (astrocytes)—Retinas and optic nerves from either C57BL/6 wild-type or Spp1 KO neonatal mice of 1–3 days old were dissociated by incubation with 0.25% trypsin and 0.01% DNase in DMEM, followed by mechanical trituration as described previously.[77,78] Dissociated cells were filtered through nylon mesh screening filters with a 52-μm pore size to efficiently remove debris. Cells were plated on polylysine-coated coverslips in DMEM/F12 with 10% FBS and then cultured at 37°C in a 95% air and 5% CO2 incubator with a change of medium twice a week. After 7–10 days in culture, the plates were shaken at 200 rpm for 18h, discarding the supernatant. This removed most of the oligodendrocytes and microglia. The remaining cells were trypsinized and passaged. After 2 rounds of trypsinization and replating, >95% of the remaining cells were positive for the astrocyte marker GFAP.

Primary cell co-culture (RGCs and astrocytes)—Confluent astrocytes were trypsinized and re-seeded in 24-well plates and further incubated for 7 days for astrocyte–neuron co-cultures as described previously.[79,80] Primary cultures of RGCs were prepared from P1-P3 C57BL/6 mice. Eyes were enucleated and retinas were dissected and placed in cold (4°C) DMEM with 100 U/ml Penicillin-Streptomycin. Retinas were cut into pieces and digested in 20 U/ml pre-warmed papain solution with 100 U/ml DNase I at 37°C for 15 min. An equal volume of 5 mg/mL ovomucoid was added to stop the reaction. Lysates were triturated several times and centrifuged at 3000 rpm for 5 min at 4°C. Cells were

resuspended in 500 μL washing buffer (0.5% BSA, 2 mM EDTA in 1× PBS). Thirty μl micro-magnetic beads conjugated Thy1.2 (CD90.2) antibody (Invitrogen, 11443D) were added into cells and incubated at 4°C for 20 min. A MACS magnetic separation system was used to isolate RGCs according to the manufacturer's instructions. The purified cells were centrifuged at 3000 rpm for 5 min at 4°C and re-suspended in culture medium (DMEM/F12 with 10%FBS, 10 mM HEPES, 2 mM L-glutamine, 100 U/ml Penicillin-Streptomycin). For the astrocyte–neuron co-cultures, astrocytes were grown to confluency and washed with phosphate-buffered saline (PBS, pH 7.4). Resuspended RGCs were seeded onto the astrocyte layer. β-III tubulin, BRN3Aand SMI32 antibodies were used to verify the purification of RGCs. At the end of the experimental period, RGCs on the astrocyte layer were fixed with 4% paraformaldehyde for 10 min and then incubated with β-tubulin. Images were taken on a SP8 confocal microscope and the length of neurites was measured using the FIJI distribution of ImageJ.[81]

METHOD DETAILS

Fluorescence-activated cell sorting—Optic nerve head was collected from Gfap-tdTomato and Spp1$^{GFPfl/fl}$GfapCre mice and digested with 0.6 mg protein/ml papain (Worthington, LS003126), 0.012 mg/ml L-cysteine(Sigma, C7352) in HBSS (Ca^{2+} and Ma^{2+} free) (Gibco, 14185-052) for 15 min at 37°C. After the incubation, tissues were centrifuged at 2000 rpm for 5 min and then removed papain/HBSS solution. Tissues were resuspended in 10% horse serum (Gibco, 26050-088) and 60 U/ml DNase I (Sigma, D-5025) in HBSS and were triturated carefully with a heat polished Pasteur pipet (World Precision Instruments, TW150-4) until all visible chunks of tissue were completely dissociated. Dissociated cells were centrifuged and resuspended in HBSS. Cell suspensions were passed through a 35-μm cell strainer into 5 mL round bottom polystyrene test tube (Falcon, 352235) for further cell sorting. Live, singlet tdTomato^{+} cells were identified as astrocytes and sorted on a FACS Aria III cell sorter (BD Biosciences) directly into collection medium. Cells sorted by FACS were centrifuged at 1000g for 10 min and cell pellets were used for further RNA extraction.

Fundus photography and optical coherence tomography—Mice were anesthetized and their pupils were dilated. Fundus images were captured using a Micron III retinal imaging system (Phoenix Research Laboratories, Pleasanton, CA). Optical coherence tomography (OCT) was performed directly after fundus photography. Anterior and posterior segment OCT images were obtained with a spectral domain OCT system (Bioptigen, Morrisville, NC). Averaged single B scans and volume scans were obtained with images centered on optic nerve head or the cornea, respectively.

Electroretinography and optomotor reflex testing—Pattern electroretinograms (PERG) were recorded from both eyes of light-adapted mice on a Celeris small animal testing system (Diagnosys LLC). PERG amplitudes were defined as the difference between the P1 peak and N2. Conventional, light-adapted ERG was recorded directly afterwards to ensure that reductions of PERG amplitudes were not due to unrelated ocular disease. The optomotor reflex was tested in awake mice that were placed on a platform in the middle of an arena made from 4 computer monitors.[82]

Retro-orbital optic nerve crush and microbead occlusion model of glaucoma —Mice were anesthetized and the intraorbital optic nerve was exposed by dissection of the conjunctiva.[83] The nerve was clamped for 10 s in the myelinated region approximately 200 μm behind the sclera using self-closing forceps. Polystyrene microbeads (15 μm diameter, Invitrogen, Carlsbad, CA, USA) were injected into the anterior chamber of the right eye through the cornea.[31,84] Control groups received an injection of sterile saline solution. Intraocular pressure was measured in both eyes with a rebound tonometer (TonoLab, iCare, Espoo, Finland) under isoflurane anesthesia. All measurements were taken in the morning to minimize circadian variation of IOP.

Tissue preparation—After euthanasia, the skull was opened, the brain was removed, and eyes and optic nerves were dissected from the surrounding tissue[85] and immediately fixed in 4% paraformaldehyde overnight. Brains were fixed separately. Eyes were hemisected along the ora serrata and the retinas were gently removed from the posterior eyecup. Four relieving cuts were made to facilitate whole-mounting of the tissue. Optic nerves were left intact and processed for sectioning. If the tissue was designed for electron microscopy, perfusion fixation was performed directly after euthanasia with 5 mL heparinized saline solution, followed by 4% paraformaldehyde solution. The tissue was dissected as described above and immediately post-fixed with 4% paraformaldehyde/0.8% glutaraldehyde in 0.5x sodium cacodylate buffer.[2,32]

Immunohistochemistry—Retinas were mounted ganglion cell side-up on nitrocellulose membranes and stained for 3 days with primary antibodies (key resources table). Optic nerves or whole brains were cryoprotected, embedded in OCT compound and sectioned at 12 μm and 30 μm, respectively, in a Leica cryostat. Sections were incubated with primary antibodies overnight at 4°C. Primary antibodies were visualized with appropriate secondary antibodies conjugated with Alexa fluorophores (Jackson ImmunoResearch and Molecular Probes). DAPI were used to counterstain nuclei. Labeled sections were mounted with Vectashield (Vector Laboratories) and imaged by confocal microscopy.

Confocal microscopy and transmission electron microscopy—Confocal image stacks were taken on a Leica SP8 confocal microscope (Leica, Wetzlar, Germany). For RGC counting, image stacks were taken through the ganglion cell layer at 0.5 μm step size and a z-projection was generated. For transmission electron microscopy, retinas and optic nerves were fixed overnight with 0.5x Karnovsky's fixative and embedded in tEPON-812 epoxy resin. Ultra-thin sections (70–90 nm) were cut from the epoxy block using a Leica EM UC7 ultramicrotome (Leica Microsystems, Buffalo Grove, IL), stained with aqueous 25% uranyl acetate replacement (Electron Microscopy Sciences, Hatfield, Pennsylvania) for 30 minutes and Sato's Lead citrate for 5 minutes, and dried using the Hiraoka grid staining technique.[32,86] Images from the retina or optic nerves were taken on a FEI Tecnai G2 Spirit transmission electron microscope (FEI, Hillsboro, Oregon) at 8o kV with an AMT XR41 digital CCD camera (Advanced Microscopy Techniques, Woburn, Massachusetts) at 400–18,500x magnification.

Paraphenylenediamine staining—The myelinated segments of optic nerves were fixed, dehydrated, and embedded in epoxy resin. Semi-thin (0.5 μm) sections were acquired using a Leica EM UC5 ultramicrotome collected on slides, and then dried on a slide warmer. Slides were stained with a solution of 1% paraphenylenediamine (PPD) in 1:1 isopropanol:methanol. Tiling images of the whole nerve were taken on an Olympus BX51 microscope Center Valley, PA, USA). The raw images were automerged using Adobe Photoshop CS6 (San Jose, CA, USA).

Axons were counted from PPD-stained optic nerve cross sections, Cell Counter function of Image J. Tiled images of optic nerves were overlaid with a grid of about 200 squares (216 μm by 216 μm) per nerve. All axons in the squares were counted to determine axon packing densities (Figure S2E). The area of the optic nerve cross section was determined by outlining its outer border using Image J. The axons number per optic nerve was calculated by axonal density and optic nerve area. Axon counts were performed by an individual blinded to the genotype of the animals and the injury induced.

cDNA synthesis and quantitative PCR—Due to the small amount of tissue from the optic nerve head, three optic nerve heads were pooled for one sample of crushed and uncrushed eyes. One well of cultured astrocytes growing in 6-well plates was one sample. After total RNA extraction using the RNeasy Plus Micro Kit (Qiagen, Valencia, CA), the purity of RNA were assessed using the NanoDrop 2000 (Thermo Fisher Scientific) and the RNA integrity was determined on the BioAnalyzer (Agilent Technologies, Santa Clara, CA). Only the RNA samples that had a 260/280 ratio >1.8 and a RNA integrity number (RIN) higher than 5 (mean RIN of 7.37 ± 0.67) were used for cDNA synthesis. Ten ng of RNA from optic nerve heads were reverse-transcribed using the Ovation qPCR System (NuGen, San Carlos, CA), and the cDNAs were diluted 1:50 as templates for quantitative PCR. GAPDH was used as a reference gene as the expression level in the optic nerve head is stable after optic nerve crush.[26] Primer sequences are given in the Table S1. At least five biological replicates were used for each condition and all samples were run in triplicate with non-template control on a StepOnePlus qPCR thermocycler (Applied Biosystems, Foster City, CA) and a Roche LightCycler 480 II (Roche Diagnostics Corporation, Indianapolis, IN).

RNA-sequencing—Total RNA was extracted from cultured astrocytes isolated from either C57BL/6 wild-type or Spp1 KO neonatal mice using the RNeasy Plus Micro Kit (Qiagen; 74034). RNA purity and integrity was examined using the NanoPhotometer spectrophotometer (IMPLEN) and the RNA Nano 6000 Assay Kit of the Bioanalyzer 2100 system (Agilent Technologies). RNA concentration was measured with Qubit RNA Assay Kit in Qubit 2.0 Fluorometer (Life Technologies). Libraries were prepared and sequenced by Novogene Sequencing was performed on an Illumina NovaSeq 6000 System, and 150-bp paired-end reads were generated.

Data analysis of RNA-seq—Reads were aligned to the mouse reference genome (GRCm38) on the computer cluster of the Harvard Chan Bioinformatics Core (HBC) using the STAR software package. Gene-expression levels were calculated using the transcripts per kilobase of exon per million fragments mapped (FPKM). All statistical analyses were

conducted using R version 4.0.5. Differential expression analysis were performed using the R package DESeq2. Genes with false-discovery-rate-adjusted p <0.05 and absolute log2 (fold change) > 0.58 found by DESeq were assigned as differentially expressed. R package ggplot2 was used for plotting MA plots. Heatmaps were generated after normalization of the raw counts using DESeq2. Functional enrichment analysis was carried out using Ingenuity Pathway Analysis (Qiagen).

Measurement of astrocyte phagocytic activity—Phagocytic activity was measured with a pHrodo Green E. coli BioParticles conjugate (catalog number P35366; Life Technologies). The particles are conjugated to pHrodo dye, the fluorescence of which increases in an acidic environment such as that of the phagosome. For measurement of phagocytic activity, astrocytes were plated onto 24-well culture plates for 3 days and incubated with pHrodo Green E. coli BioParticles (Invitrogen, P35366) for 4 hours. Phagocytic activity was determined based on the fluorescence intensity of the cells by confocal microscopy.

Phagocytic activity was also measured by spectrophotometry. Plate astrocytes into a 96-well plate as experimental wells. Leave two wells empty of cells for every control well, so that a no-cell control background subtraction may be performed. Astrocytes were cultured for 24 h, and the culture medium was then replaced with 200 μL of pHrodo Green E. coli BioParticles conjugate solution in experimental and no-cell control wells. Cover and transfer the microplate to an incubator warmed to 37°C for 4 hours to allow phagocytosis and acidification to reach its maximum. Scan all experimental and no-cell control wells of the microplate in the fluorescence plate reader (BioTek Synergy H1 instrument). Phagocytic activity was determined based on relative fluorescence intensity of pHrodo particles in astrocytes.

Measurement of mitochondrial respiration—Astrocytes were counted and plated at 2.0×10^4 (C57BL/6 astrocytes) or 1.0×10^4 (Spp1 KO astrocytes) cells per well in a Seahorse XF24 Cell Culture Microplate for all experiments (Agilent) 3 days before the experiments. Cells were then treated with rSPP1 or Vdac1 siRNA or Metformin in each experiment for 24 h. Cells were washed twice and pre-incubated with Agilent Seahorse XF medium (Agilent) supplemented with 25 mM D-glucose, 2 mM L-glutamine and 1 mM sodium pyruvate for 1 h at 37°C in an incubator without CO2 regulation. A final volume of 500 μL was placed in each well. For OCR and ECAR mitochondrial stress test experiments, cells were treated with 1.5 μM oligomycin (an ATP synthase inhibitor), 1 μM carbonyl cyanide 4-(trifluoromethoxy) phenylhydrazone (FCCP, a mitochondrial uncoupler) and 2.0 μM rotenone plus 2.0 μM antimycin A (complex I and III inhibitors). As proliferation and cell growth may vary after plating, protein concentration was quantified by the bicinchoninic acid (BCA) assay to normalize the OCR.[87–89]

Visualization of cytosolic ATP—Plasmid GfaABC1D-cyto-Ruby3-iATPSnFR1.0 was developed by the laboratory of Baljit Khakh and expresses cytoplasmic ATP sensor in astrocytes with red reference protein.[44] Plasmid #102554 was purchased from Addgene. Bacteria containing the plasmid was amplified in LB medium with ampicillin and the plasmid was extracted using the EndoFree Plasmid Maxi Kit (QIAGEN, #12362).

Astrocytes at 70–90% confluency were transfected with the plasmid and Lipofectamine 3000. The transfection of a single well of a 24-well dish was as following: 1 μg of DNA and 2 μL P3000 were added to one tube containing 50 μL of Opti-MEM and 3 μL of Lipofectamine 3000 was added to the other tube containing 50 μL of Opti-MEM. The content of the two tubes was mixed and incubated for 20 min at room temperature, and 400 μL of fresh complete medium were added into the DNA-lipid complexes mixture before adding the mixture to astrocytes. The medium was changed the following day. Cells were incubated for 2–4 days at 37°C before fixation with 4% PFA. Images were taken on SP8 confocal microscope.

siRNA knockdown—CD44 siRNA (165814), Integrin alpha 5 siRNA (67718), Vdac1 siRNA (187532) and Silencer® Negative Control #1 siRNA (AM4611) were obtained from Thermo Fisher Scientific. siRNA were resuspended at 50 μM. Lipofectamine 3000 transfection reagent (ThermoFisher Scientific) was used to transfect siRNA into astrocytes according to the manufacturer's instructions. Astrocytes were grown in DMEM/F-12 complete media with siRNA (50 nM) and incubated for 24–72 h after treatment. Reagents are summarized in the key resources table.

Astrocyte migration and phagocytosis assays—The astrocytes after first passage cultured for seven days and were transferred to a 6-well plate coated with poly-L-lysine and then the scratch injury model in cultured astrocytes was performed as described previously.[90,91] Briefly, the cultured astrocytes were scratched with a 200 μL pipette tip 2 times in the same direction. The sham group was suffered the same operation described above, but kept the tip from touching the astrocytes. The multiwell plates containing astrocytes were washed once with PBS to remove the debris and incubated with fresh media. Immediately following the addition of treatments (day 1), pictures were taken using an inverted microscope in bright field (Leica DMi8). Astrocytes were maintained after the scratch and pictures were taken at day 3 and 5. Individual images were stitched to reconstruct the scratch at time day 1, 3 and 5 and the cell-free area was calculated using ImageJ to estimate the wound closure. For measurement of phagocytic activity, astrocytes were plated onto 24-well culture plates for 3 days, and incubated with pHrodo Green E. coli BioParticles (Invitrogen, P35366) for 4 hours. Phagocytic activity was determined based on the fluorescence intensity of the cells by using a BioTek instrument.

AAV2-mediated gene transfer—The coding region of Spp1, followed by a cleavable F2A linker region and the EGFP gene was synthetized (Integrated DNA Technologies, Coralville, IA), inserted into the AAV2 backbone plasmid, sequenced, and used to generate the virus (1.41E12 GC/ml, Viral Vector Core, MEEI). AAV2 expressing only EGFP served as a control. In both constructs, gene expression is driven by the CMV promoter. One μl of AAV2-Spp1-EGFP or control virus was injected intravitreally, and transfection efficiency was monitored by fundus photography and immunohistochemistry.

Intravitreal delivery of a slow-release SPP1 protein (SPP1 PODS)—Mice were injected intravitreally with 1μL of slow-release SPP1 PODS (500 ng/mL) in the same setting

when microbeads were injected into eyes. SPP1 PODS were administered once again one week later. Mice were killed and their tissue harvested on day 14 after microbeads injection.

QUANTIFICATION AND STATISTICAL ANALYSIS

Statistical significance was performed with GraphPad Prism 8. The data are provided as mean ± SEM. Data were analyzed using an unpaired two-tailed Student's t test for comparisons of two groups. For comparison of multiple groups, normally distributed data were assessed using a one-way ANOVA with Tukey's post-test. For bivariate comparisons, a two-way ANOVA with Bonferroni's post-test was used. Differences were considered statistically significant at $p < 0.05$. Differential gene expression (DGE) analysis was done using R 4.0.5 and RStudio 1.3.1056. Cumulative IOPs were calculated using Matlab. Figures were prepared using Adobe Photoshop CS6. The graphical abstract was prepared using BioRender.

Supplementary Material

Refer to Web version on PubMed Central for supplementary material.

ACKNOWLEDGMENTS

We thank D. Sun, P. d'Amore, and K. Sweadner for critically reading the manuscript; D. Shu and M. Saint-Geniez for help with the Seahorse Bioanalyzer; and P. Seifert for help with tissue preparation and transmission electron microscopy. This work was supported by NIH grant R01 EY19703, NIH Core Grant for Vision Research P30EY003790, and a Shaffer grant of the Glaucoma Research Foundation.

REFERENCES

1. Calkins DJ (2013). Age-related changes in the visual pathways: blame it on the axon. Invest. Ophthalmol. Vis. Sci. 54, ORSF37–41. 10.1167/iovs.13-12784. [PubMed: 24335066]
2. Zhu Y, Pappas AC, Wang R, Seifert P, Sun D, and Jakobs TC (2018). Ultrastructural morphology of the optic nerve head in aged and glaucomatous mice. Invest. Ophthalmol. Vis. Sci. 59, 3984–3996. 10.1167/iovs.18-23885. [PubMed: 30098187]
3. Tham YC, Li X, Wong TY, Quigley HA, Aung T, and Cheng CY (2014). Global prevalence of glaucoma and projections of glaucoma burden through 2040: a systematic review and meta-analysis. Ophthalmology 121, 2081–2090. 10.1016/j.ophtha.2014.05.013. [PubMed: 24974815]
4. Keenan TDL, Cukras CA, and Chew EY (2021). Age-related macular degeneration: epidemiology and clinical aspects. Adv. Exp. Med. Biol. 1256, 1–31. 10.1007/978-3-030-66014-7_1. [PubMed: 33847996]
5. Blasiak J (2020). Senescence in the pathogenesis of age-related macular degeneration. Cell. Mol. Life Sci. 77, 789–805. 10.1007/s00018-019-03420-x. [PubMed: 31897543]
6. Quigley HA (2011). Glaucoma. Lancet 377, 1367–1377. 10.1016/S0140-6736. [PubMed: 21453963]
7. Lu Y, Brommer B, Tian X, Krishnan A, Meer M, Wang C, Vera DL, Zeng Q, Yu D, Bonkowski MS, et al. (2020). Reprogramming to recover youthful epigenetic information and restore vision. Nature 588, 124–129. 10.1038/s41586-020-2975-4. [PubMed: 33268865]
8. Meszaros A, Molnar K, Nogradi B, Hernadi Z, Nyul-Toth A, Wilhelm I, and Krizbai IA (2020). Neurovascular inflammaging in health and disease. Cells 9, 1614. 10.3390/cells9071614. [PubMed: 32635451]
9. Chrysostomou V, Galic S, van Wijngaarden P, Trounce IA, Steinberg GR, and Crowston JG (2016). Exercise reverses age-related vulnerability of the retina to injury by preventing complement-

mediated synapse elimination via a BDNF-dependent pathway. Aging Cell 15, 1082–1091. 10.1111/acel.12512. [PubMed: 27613664]

10. Tribble JR, Hui F, Joe M, Bell K, Chrysostomou V, Crowston JG, and Williams PA (2021). Targeting diet and exercise for neuroprotection and neurorecovery in glaucoma. Cells 10, 295. 10.3390/cells10020295. [PubMed: 33535578]
11. Preininger MK, and Kaufer D (2022). Blood-brain barrier dysfunction and astrocyte senescence as reciprocal drivers of neuropathology in aging. Int. J. Mol. Sci. 23, 6217. 10.3390/ijms23116217. [PubMed: 35682895]
12. Behfar Q, Ramirez Zuniga A, and Martino-Adami PV (2022). Aging, senescence, and dementia. J. Prev. Alzheimers Dis. 9, 523–531. 10.14283/jpad.2022.42. [PubMed: 35841253]
13. Lee J, Kim SW, and Kim KT (2022). Region-specific characteristics of astrocytes and microglia: a possible involvement in aging and diseases. Cells 11, 1902. 10.3390/cells11121902. [PubMed: 35741031]
14. Boisvert MM, Erikson GA, Shokhirev MN, and Allen NJ (2018). The aging astrocyte transcriptome from multiple regions of the mouse brain. Cell Rep. 22, 269–285. 10.1016/j.celrep.2017.12.039. [PubMed: 29298427]
15. Clarke LE, Liddelow SA, Chakraborty C, Münch AE, Heiman M, and Barres BA (2018). Normal aging induces A1-like astrocyte reactivity. Proc. Natl. Acad. Sci. USA 115, E1896–E1905. 10.1073/pnas.1800165115. [PubMed: 29437957]
16. Palmer AL, and Ousman SS (2018). Astrocytes and aging. Front. Aging Neurosci. 10, 337. 10.3389/fnagi.2018.00337. [PubMed: 30416441]
17. Morcos Y, and Chan-Ling T (2000). Concentration of astrocytic filaments at the retinal optic nerve junction is coincident with the absence of intra-retinal myelination: comparative and developmental evidence. J. Neurocytol. 29, 665–678. [PubMed: 11353290]
18. Sun D, Lye-Barthel M, Masland RH, and Jakobs TC (2009). The morphology and spatial arrangement of astrocytes in the optic nerve head of the mouse. J. Comp. Neurol. 516, 1–19. 10.1002/cne.22058. [PubMed: 19562764]
19. Davis C.h.O., Kim KY, Bushong EA, Mills EA, Boassa D, Shih T, Kinebuchi M, Phan S, Zhou Y, Bihlmeyer NA, et al. (2014). Transcellular degradation of axonal mitochondria. Proc. Natl. Acad. Sci. USA 111, 9633–9638. 10.1073/pnas.1404651111. [PubMed: 24979790]
20. Sun D, Moore S, and Jakobs TC (2017). Optic nerve astrocyte reactivity protects function in experimental glaucoma and other nerve injuries. J. Exp. Med. 214, 1411–1430. 10.1084/jem.20160412. [PubMed: 28416649]
21. Johnson EC, Jia L, Cepurna WO, Doser TA, and Morrison JC (2007). Global changes in optic nerve head gene expression after exposure to elevated intraocular pressure in a rat glaucoma model. Invest. Ophthalmol. Vis. Sci. 48, 3161–3177. 10.1167/iovs.06-1282. [PubMed: 17591886]
22. Johnson EC, Doser TA, Cepurna WO, Dyck JA, Jia L, Guo Y, Lambert WS, and Morrison JC (2011). Cell proliferation and interleukin-6-type cytokine signaling are implicated by gene expression responses in early optic nerve head injury in rat glaucoma. Invest. Ophthalmol. Vis. Sci. 52, 504–518. 10.1167/iovs.10-5317. [PubMed: 20847120]
23. Howell GR, Macalinao DG, Sousa GL, Walden M, Soto I, Kneel- and SC, Barbay JM, King BL, Marchant JK, Hibbs M, et al. (2011). Molecular clustering identifies complement and endothelin induction as early events in a mouse model of glaucoma. J. Clin. Invest. 121, 1429–1444. 10.1172/JCI44646. [PubMed: 21383504]
24. Howell GR, Soto I, Zhu X, Ryan M, Macalinao DG, Sousa GL, Caddle LB, MacNicoll KH, Barbay JM, Porciatti V, et al. (2012). Radiation treatment inhibits monocyte entry into the optic nerve head and prevents neuronal damage in a mouse model of glaucoma. J. Clin. Invest. 122, 1246–1261. 10.1172/JCI61135. [PubMed: 22426214]
25. Zamanian JL, Xu L, Foo LC, Nouri N, Zhou L, Giffard RG, and Barres BA (2012). Genomic analysis of reactive astrogliosis. J. Neurosci. 32, 6391–6410. 10.1523/JNEUROSCI.6221-11.2012. [PubMed: 22553043]
26. Qu J, and Jakobs TC (2013). The time course of gene expression during reactive gliosis in the optic nerve. PLoS One 8, e67094. 10.1371/journal.pone.0067094. [PubMed: 23826199]

27. Hullinger TG, Pan Q, Viswanathan HL, and Somerman MJ (2001). TGFbeta and BMP-2 activation of the OPN promoter: roles of smad- and hox-binding elements. Exp. Cell Res. 262, 69–74. 10.1006/excr.2000.5074. [PubMed: 11120606]
28. Liu YN, Kang BB, and Chen JH (2004). Transcriptional regulation of human osteopontin promoter by C/EBPalpha and AML-1 in metastatic cancer cells. Oncogene 23, 278–288. 10.1038/sj.onc.1207022. [PubMed: 14712233]
29. Jakobs TC (2014). Differential gene expression in glaucoma. Cold Spring Harb. Perspect. Med. 4, a020636. 10.1101/cshperspect.a020636a020636. [PubMed: 24985133]
30. Ruzafa N, Pereiro X, Aspichueta P, Araiz J, and Vecino E (2018). The retina of osteopontin deficient mice in aging. Mol. Neurobiol. 55, 213–221. 10.1007/s12035-017-0734-9. [PubMed: 28866734]
31. Sappington RM, Carlson BJ, Crish SD, and Calkins DJ (2010). The microbead occlusion model: a paradigm for induced ocular hypertension in rats and mice. Invest. Ophthalmol. Vis. Sci. 51, 207–216. 10.1167/iovs.09-3947. [PubMed: 19850836]
32. Wang R, Seifert P, and Jakobs TC (2017). Astrocytes in the optic nerve head of glaucomatous mice display a characteristic reactive phenotype. Invest. Ophthalmol. Vis. Sci. 58, 924–932. 10.1167/iovs.16-20571. [PubMed: 28170536]
33. Krishnan A, Kocab AJ, Zacks DN, Marshak-Rothstein A, and Gregory-Ksander M (2019). A small peptide antagonist of the Fas receptor inhibits neuroinflammation and prevents axon degeneration and retinal ganglion cell death in an inducible mouse model of glaucoma. J. Neuroinflammation 16, 184. 10.1186/s12974-019-1576-3. [PubMed: 31570110]
34. Weishaupt JH, Klöcker N, and Bähr M (2005). Axotomy-induced early down-regulation of POU-IV class transcription factors Brn-3a and Brn-3b in retinal ganglion cells. J. Mol. Neurosci. 26, 17–25. 10.1385/JMN:26:1:017. [PubMed: 15968082]
35. Buckingham BP, Inman DM, Lambert W, Oglesby E, Calkins DJ, Steele MR, Vetter ML, Marsh-Armstrong N, and Horner PJ (2008). Progressive ganglion cell degeneration precedes neuronal loss in a mouse model of glaucoma. J. Neurosci. 28, 2735–2744. 10.1523/JNEUROSCI.4443-07.2008. [PubMed: 18337403]
36. Pelzel HR, Schlamp CL, and Nickells RW (2010). Histone H4 deacetylation plays a critical role in early gene silencing during neuronal apoptosis. BMC Neurosci. 11, 62. 10.1186/1471-2202-11-62. [PubMed: 20504333]
37. Berkelaar M, Clarke DB, Wang YC, Bray GM, and Aguayo AJ (1994). Axotomy results in delayed death and apoptosis of retinal ganglion cells in adult rats. J. Neurosci. 14, 4368–4374. [PubMed: 8027784]
38. Duan X, Qiao M, Bei F, Kim IJ, He Z, and Sanes JR (2015). Subtype-specific regeneration of retinal ganglion cells following axotomy: effects of osteopontin and mTOR signaling. Neuron 85, 1244–1256. 10.1016/j.neuron.2015.02.017. [PubMed: 25754821]
39. Foo LC, Allen NJ, Bushong EA, Ventura PB, Chung WS, Zhou L, Cahoy JD, Daneman R, Zong H, Ellisman MH, and Barres BA (2011). Development of a method for the purification and culture of rodent astrocytes. Neuron 71, 799–811. 10.1016/j.neuron.2011.07.022. [PubMed: 21903074]
40. Liddelow SA, Guttenplan KA, Clarke LE, Bennett FC, Bohlen CJ, Schirmer L, Bennett ML, Münch AE, Chung WS, Peterson TC, et al. (2017). Neurotoxic reactive astrocytes are induced by activated microglia. Nature 541, 481–487. 10.1038/nature21029. [PubMed: 28099414]
41. Nguyen JV, Soto I, Kim KY, Bushong EA, Oglesby E, Valiente-Soriano FJ, Yang Z, Davis C.h.O., Bedont JL, Son JL, et al. (2011). Myelination transition zone astrocytes are constitutively phagocytic and have synuclein dependent reactivity in glaucoma. Proc. Natl. Acad. Sci. USA 108, 1176–1181. 10.1073/pnas.1013965108. [PubMed: 21199938]
42. Iram T, Ramirez-Ortiz Z, Byrne MH, Coleman UA, Kingery ND, Means TK, Frenkel D, and El Khoury J (2016). Megf10 is a receptor for C1Q that mediates clearance of apoptotic cells by astrocytes. J. Neurosci. 36, 5185–5192. 10.1523/JNEUROSCI.3850-15.2016. [PubMed: 27170117]
43. Ahmed M, and Kundu GC (2010). Osteopontin selectively regulates p70S6K/mTOR phosphorylation leading to NF-kappaB dependent AP-1-mediated ICAM-1 expression in breast cancer cells. Mol. Cancer 9, 101. 10.1186/1476-4598-9-101. [PubMed: 20459645]

44. Lobas MA, Tao R, Nagai J, Kronschläger MT, Borden PM, Marvin JS, Looger LL, and Khakh BS (2019). A genetically encoded single-wavelength sensor for imaging cytosolic and cell surface ATP. Nat. Commun. 10, 711. 10.1038/s41467-019-08441-5. [PubMed: 30755613]
45. Sanes JR, and Masland RH (2015). The types of retinal ganglion cells: current status and implications for neuronal classification. Annu. Rev. Neurosci. 38, 221–246. 10.1146/annurev-neuro-071714-034120. [PubMed: 25897874]
46. Sofroniew MV (2015). Astrogliosis. Cold Spring Harb. Perspect. Biol. 7, a020420. 10.1101/cshperspect.a020420.
47. Escartin C, Galea E, Lakatos A, O'Callaghan JP, Petzold GC, Serrano-Pozo A, Steinhäuser C, Volterra A, Carmignoto G, Agarwal A, et al. (2021). Reactive astrocyte nomenclature, definitions, and future directions. Nat. Neurosci. 24, 312–325. 10.1038/s41593-020-00783-4. [PubMed: 33589835]
48. Sun D, Qu J, and Jakobs TC (2013). Reversible reactivity by optic nerve astrocytes. Glia 61, 1218–1235. 10.1002/glia.22507. [PubMed: 23650091]
49. Das S, Li Z, Noori A, Hyman BT, and Serrano-Pozo A (2020). Meta-analysis of mouse transcriptomic studies supports a context-dependent astrocyte reaction in acute CNS injury versus neurodegeneration. J. Neuroinflammation 17, 227. 10.1186/s12974-020-01898-y. [PubMed: 32736565]
50. Habib N, McCabe C, Medina S, Varshavsky M, Kitsberg D, Dvir-Szternfeld R, Green G, Dionne D, Nguyen L, Marshall JL, et al. (2020). Disease-associated astrocytes in Alzheimer's disease and aging. Nat. Neurosci. 23, 701–706. 10.1038/s41593-020-0624-8. [PubMed: 32341542]
51. Clarke BE, Taha DM, Tyzack GE, and Patani R (2021). Regionally encoded functional heterogeneity of astrocytes in health and disease: a perspective. Glia 69, 20–27. 10.1002/glia.23877. [PubMed: 32749770]
52. Bouvier DS, Fixemer S, Heurtaux T, Jeannelle F, Frauenknecht KBM, and Mittelbronn M (2022). The multifaceted neurotoxicity of astrocytes in ageing and age-related neurodegenerative diseases: a sranslational perspective. Front. Physiol. 13, 814889. 10.3389/fphys.2022.814889. [PubMed: 35370777]
53. Picca A, Ferri E, Calvani R, Coelho-Júnior HJ, Marzetti E, and Arosio B (2022). Age-associated glia remodeling and mitochondrial dysfunction in neurodegeneration: antioxidant supplementation as a possible intervention. Nutrients 14, 2406. 10.3390/nu14122406. [PubMed: 35745134]
54. Rutigliani C, Tribble JR, Hagström A, Lardner E, Jóhannesson G, Stålhammar G, and Williams PA (2022). Widespread retina and optic nerve neuroinflammation in enucleated eyes from glaucoma patients. Acta Neuropathol. Commun. 10, 118. 10.1186/s40478-022-01427-3. [PubMed: 35986368]
55. Fernández-Albarral JA, Salazar JJ, de Hoz R, Marco EM, Martín-Sánchez B, Flores-Salguero E, Salobrar-García E, López-Cuenca I, Barrios-Sabador V, Avilés-Trigueros M, et al. (2021). Retinal molecular changes are associated with neuroinflammation and loss of RGCs in an experimental model of glaucoma. Int. J. Mol. Sci. 22, 2066. 10.3390/ijms22042066. [PubMed: 33669765]
56. Mathew DJ, Livne-Bar I, and Sivak JM (2021). An inducible rodent glaucoma model that exhibits gradual sustained increase in intraocular pressure with distinct inner retina and optic nerve inflammation. Sci. Rep. 11, 22880. 10.1038/s41598-021-02057-w. [PubMed: 34819548]
57. Tonner H, Hunn S, Auler N, Schmelter C, Beutgen VM, von Pein HD, Pfeiffer N, and Grus FH (2022). A sonoclonal anti-HMGB1 antibody attenuates neurodegeneration in an experimental animal model of glaucoma. Int. J. Mol. Sci. 23, 4107. 10.3390/ijms23084107. [PubMed: 35456925]
58. López-Teros M, Alarcón-Aguilar A, López-Diazguerrero NE, Luna-López A, and Königsberg M (2022). Contribution of senescent and reactive astrocytes on central nervous system inflammaging. Biogerontology 23, 21–33. 10.1007/s10522-022-09952-3. [PubMed: 35084630]
59. Borregaard N, and Herlin T (1982). Energy metabolism of human neutrophils during phagocytosis. J. Clin. Invest. 70, 550–557. 10.1172/jci110647. [PubMed: 7107894]
60. Davis CHO, and Marsh-Armstrong N (2014). Discovery and implications of transcellular mitophagy. Autophagy 10, 2383–2384. 10.4161/15548627.2014.981920. [PubMed: 25484086]

61. Honda S, Namekata K, Kimura A, Guo X, Harada C, Murakami A, Matsuda A, and Harada T (2019). Survival of alpha and intrinsically photosensitive retinal ganglion cells in NMDA-induced neurotoxicity and a mouse model of normal gension glaucoma. Invest. Ophthalmol. Vis. Sci. 60, 3696–3707. 10.1167/iovs.19-27145. [PubMed: 31487370]

62. Hammond TR, Dufort C, Dissing-Olesen L, Giera S, Young A, Wysoker A, Walker AJ, Gergits F, Segel M, Nemesh J, et al. (2019). Single-cell RNA sequencing of microglia throughout the mouse lifespan and in the injured brain reveals complex cell-state changes. Immunity 50, 253–271.e6. 10.1016/j.immuni.2018.11.004. [PubMed: 30471926]

63. Lee SH, Park YS, Paik SS, and Kim IB (2021). Differential response of muller cells and microglia in a mouse retinal detachment model and its implications in metached and non-detached regions. Cells 10, 1972. 10.3390/cells10081972. [PubMed: 34440741]

64. Ruzafa N, Pereiro X, Lepper MF, Hauck SM, and Vecino E (2018). A proteomics approach to identify candidate proteins secreted by muller glia that protect ganglion cells in the retina. Proteomics 18, e1700321. 10.1002/pmic.201700321. [PubMed: 29645351]

65. Del Río P, Irmler M, Arango-González B, Favor J, Bobe C, Bartsch U, Vecino E, Beckers J, Hauck SM, and Ueffing M (2011). GDNF-induced osteopontin from Muller glial cells promotes photoreceptor survival in the Pde6brd1 mouse model of retinal degeneration. Glia 59, 821–832. 10.1002/glia.21155. [PubMed: 21360756]

66. Dinice L, Cacciamani A, Esposito G, Taurone S, Carletti R, Ripandelli G, Artico M, and Micera A (2020). Osteopontin in vitreous and idiopathic epiretinal membranes. Graefes Arch. Clin. Exp. Ophthalmol. 258, 1503–1513. 10.1007/s00417-020-04685-w. [PubMed: 32277255]

67. Weinreb RN, Aung T, and Medeiros FA (2014). The pathophysiology and treatment of glaucoma: a review. JAMA 311, 1901–1911. 10.1001/jama.2014.3192. [PubMed: 24825645]

68. Robertson JV, Golesic E, Gauldie J, and West-Mays JA (2010). Ocular gene transfer of active TGF-beta induces changes in anterior segment morphology and elevated IOP in rats. Invest. Ophthalmol. Vis. Sci. 51, 308–318. 10.1167/iovs.09-3380. [PubMed: 19696167]

69. Lam JD, Oh DJ, Wong LL, Amarnani D, Park-Windhol C, Sanchez AV, Cardona-Velez J, McGuone D, Stemmer-Rachamimov AO, Eliott D, et al. (2017). Identification of RUNX1 as a mediator of aberrant retinal angiogenesis. Diabetes 66, 1950–1956. 10.2337/db16-1035. [PubMed: 28400392]

70. Bennett J, Wellman J, Marshall KA, McCague S, Ashtari M, DiStefano-Pappas J, Elci OU, Chung DC, Sun J, Wright JF, et al. (2016). Safety and durability of effect of contralateral-eye administration of AAV2 gene therapy in patients with childhood-onset blindness caused by RPE65 mutations: a follow-on phase 1 trial. Lancet 388, 661–672. 10.1016/S0140-6736(16)30371-3. [PubMed: 27375040]

71. Russell S, Bennett J, Wellman JA, Chung DC, Yu ZF, Tillman A, Wittes J, Pappas J, Elci O, McCague S, et al. (2017). Efficacy and safety of voretigene neparvovec (AAV2-hRPE65v2) in patients with RPE65-mediated inherited retinal dystrophy: a randomised, controlled, open-label, phase 3 trial. Lancet 390, 849–860. 10.1016/S0140-6736(17)31868-8. [PubMed: 28712537]

72. Wójcik-Gryciuk A, Gajewska-Woźniak O, Kordecka K, Boguszewski PM, Waleszczyk W, and Skup M (2020). Neuroprotection of retinal ganglion cells with AAV2-BDNF pretreatment restoring normal TrkB receptor protein levels in glaucoma. Int. J. Mol. Sci. 21, 6262. 10.3390/ijms21176262. [PubMed: 32872441]

73. Jacobson SG, Cideciyan AV, Ratnakaram R, Heon E, Schwartz SB, Roman AJ, Peden MC, Aleman TS, Boye SL, Sumaroka A, et al. (2012). Gene therapy for leber congenital amaurosis caused by RPE65 mutations: safety and efficacy in 15 children and adults followed up to 3 years. Arch. Ophthalmol. 130, 9–24. 10.1001/archophthalmol.2011.298. [PubMed: 21911650]

74. Simonelli F, Maguire AM, Testa F, Pierce EA, Mingozzi F, Bennicelli JL, Rossi S, Marshall K, Banfi S, Surace EM, et al. (2010). Gene therapy for Leber's congenital amaurosis is safe and effective through 1.5 years after vector administration. Mol. Ther. 18, 643–650. 10.1038/mt.2009.277. [PubMed: 19953081]

75. Jacobson SG, Cideciyan AV, Ho AC, Peshenko IV, Garafalo AV, Roman AJ, Sumaroka A, Wu V, Krishnan AK, Sheplock R, et al. (2021). Safety and improved efficacy signals following gene therapy in childhood blindness caused by GUCY2D mutations. iScience 24, 102409. 10.1016/j.isci.2021.102409. [PubMed: 33997691]

76. Kuzmin DA, Shutova MV, Johnston NR, Smith OP, Fedorin VV, Kukushkin YS, van der Loo JCM, and Johnstone EC (2021). The clinical landscape for AAV gene therapies. Nat. Rev. Drug Discov. 20, 173–174. 10.1038/d41573-021-00017-7. [PubMed: 33495615]
77. Li S, Cai J, Feng ZB, Jin ZR, Liu BH, Zhao HY, Jing HB, Wei TJ, Yang GN, Liu LY, et al. (2017). BDNF contributes to spinal long-term potentiation and mechanical hypersensitivity via Fyn-mediated phosphorylation of NMDA receptor GluN2B subunit at tyrosine 1472 in rats following spinal nerve ligation. Neurochem. Res. 42, 2712–2729. 10.1007/s11064-017-2274-0. [PubMed: 28497343]
78. Yang Y, Li S, Jin ZR, Jing HB, Zhao HY, Liu BH, Liang YJ, Liu LY, Cai J, Wan Y, and Xing GG (2018). Decreased abundance of TRESK two-pore domain potassium channels in sensory neurons underlies the pain associated with bone metastasis. Sci. Signal. 11, eaao5150. 10.1126/scisignal.aao5150. [PubMed: 30327410]
79. Jimenez-Blasco D, Busquets-Garcia A, Hebert-Chatelain E, Serrat R, Vicente-Gutierrez C, Ioannidou C, Gómez-Sotres P, Lopez-Fabuel I, Resch-Beusher M, Resel E, et al. (2020). Glucose metabolism links astroglial mitochondria to cannabinoid effects. Nature 583, 603–608. 10.1038/s41586-020-2470-y. [PubMed: 32641832]
80. Ma J, Guo C, Guo C, Sun Y, Liao T, Beattie U, López FJ, Chen DF, and Lashkari K (2015). Transplantation of human neural progenitor cells expressing IGF-1 enhances retinal ganglion cell survival. PLoS One 10, e0125695. 10.1371/journal.pone.0125695. [PubMed: 25923430]
81. Schindelin J, Arganda-Carreras I, Frise E, Kaynig V, Longair M, Pietzsch T, Preibisch S, Rueden C, Saalfeld S, Schmid B, et al. (2012). Fiji: an open-source platform for biological-image analysis. Nat. Methods 9, 676–682. 10.1038/nmeth.2019. [PubMed: 22743772]
82. Gao S, and Jakobs TC (2016). Mice homozygous for a deletion in the glaucoma susceptibility locus INK4 show increased vulnerability of retinal ganglion cells to elevated intraocular pressure. Am. J. Pathol. 186, 985–1005. 10.1016/j.ajpath.2015.11.026. [PubMed: 26883755]
83. Sun D, Lye-Barthel M, Masland RH, and Jakobs TC (2010). Structural remodeling of fibrous astrocytes after axonal injury. J. Neurosci. 30, 14008–14019. 10.1523/JNEUROSCI.3605-10.2010. [PubMed: 20962222]
84. Chen H, Wei X, Cho KS, Chen G, Sappington R, Calkins DJ, and Chen DF (2011). Optic neuropathy due to microbead-induced elevated intraocular pressure in the mouse. Invest. Ophthalmol. Vis. Sci. 52, 36–44. 10.1167/iovs.09-5115. [PubMed: 20702815]
85. Jakobs TC, Libby RT, Ben Y, John SWM, and Masland RH (2005). Retinal ganglion cell degeneration is topological but not cell type specific in DBA/2J mice. J. Cell Biol. 171, 313–325. 10.1083/jcb.200506099. [PubMed: 16247030]
86. Seifert P (2017). Modified Hiraoka TEM grid staining apparatus and technique using 3D printed materials and gadolinium triacetate tetrahydrate, a non-radioactive uranyl acetate substitute. J. Histotechnol. 40, 130–135. 10.1080/01478885.2017.1361117. [PubMed: 31105361]
87. Minhas PS, Latif-Hernandez A, McReynolds MR, Durairaj AS, Wang Q, Rubin A, Joshi AU, He JQ, Gauba E, Liu L, et al. (2021). Restoring metabolism of myeloid cells reverses cognitive decline in ageing. Nature 590, 122–128. 10.1038/s41586-020-03160-0. [PubMed: 33473210]
88. Hernansanz-Agustín P, Choya-Foces C, Carregal-Romero S, Ramos E, Oliva T, Villa-Piña T, Moreno L, Izquierdo-Álvarez A, Cabrera-García JD, Cortés A, et al. (2020). Na(+) controls hypoxic signalling by the mitochondrial respiratory chain. Nature 586, 287–291. 10.1038/s41586-020-2551-y. [PubMed: 32728214]
89. Luongo TS, Eller JM, Lu MJ, Niere M, Raith F, Perry C, Bornstein MR, Oliphint P, Wang L, McReynolds MR, et al. (2020). SLC25A51 is a mammalian mitochondrial NAD(+) transporter. Nature 588, 174–179. 10.1038/s41586-020-2741-7. [PubMed: 32906142]
90. Li D, Liu N, Zhao HH, Zhang X, Kawano H, Liu L, Zhao L, and Li HP (2017). Interactions between Sirt1 and MAPKs regulate astrocyte activation induced by brain injury in vitro and in vivo. J. Neuroinflammation 14, 67. 10.1186/s12974-017-0841-6. [PubMed: 28356158]
91. Gao K, Wang CR, Jiang F, Wong AYK, Su N, Jiang JH, Chai RC, Vatcher G, Teng J, Chen J, et al. (2013). Traumatic scratch injury in astrocytes triggers calcium influx to activate the JNK/c-Jun/AP-1 pathway and switch on GFAP expression. Glia 61, 2063–2077. 10.1002/glia.22577. [PubMed: 24123203]

Highlights

- Loss of astrocytic SPP1 increases retinal ganglion cell vulnerability to injury
- SPP1 expression in astrocytes is regulated by TGF-β1, RUNX1, and E2F1
- SPP1 increases mitochondrial function and phagocytosis
- SPP1 overexpression protects retinal ganglion cells and preserves visual function

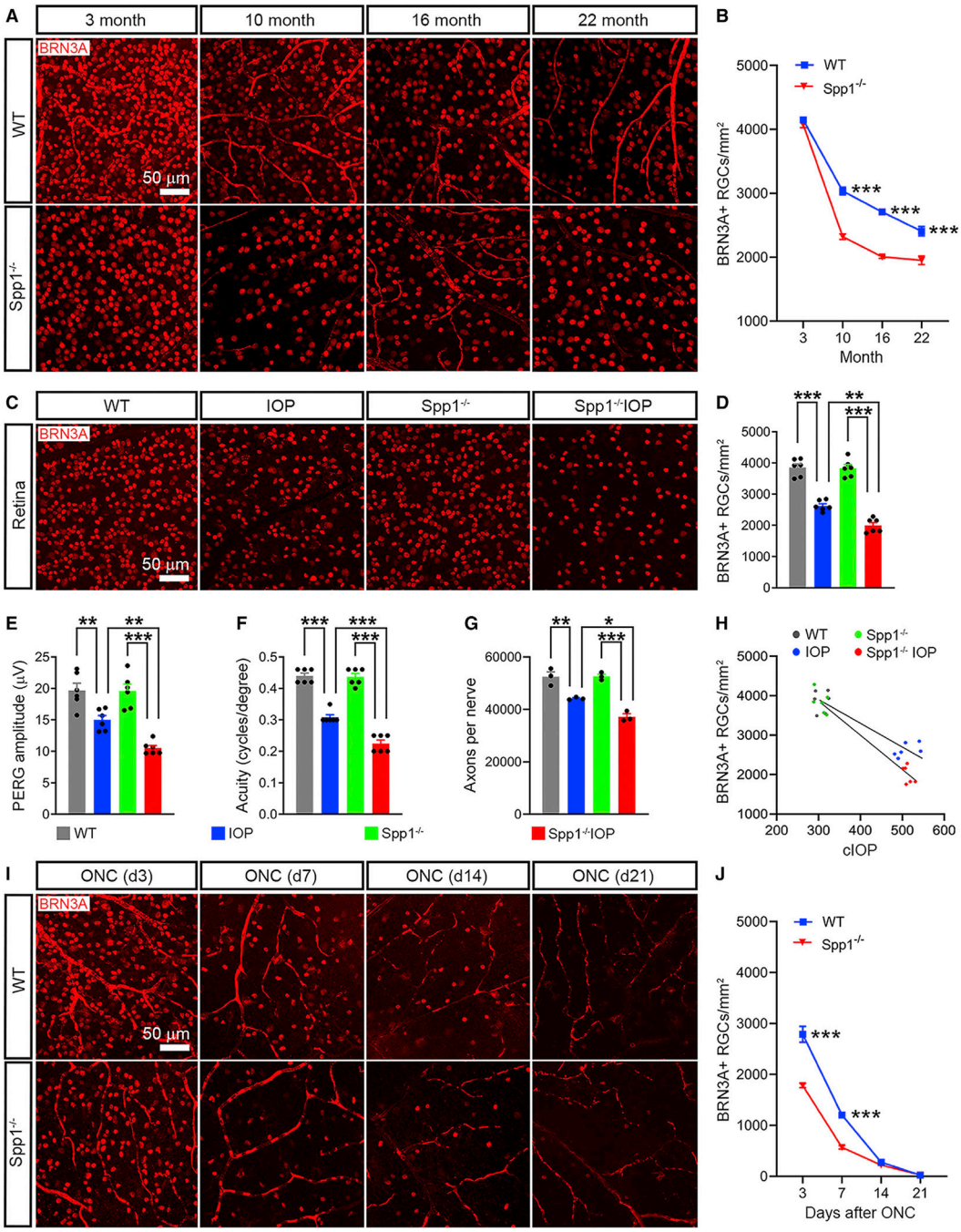

Figure 1. SPP1 protects against RGCs loss and vision decline in aging, glaucoma, and traumatic optic injury

(A) BRN3A-labeled RGCs in wild-type (WT; C57BL/6) and *Spp1*$^{-/-}$ (Spp1 KO) mice at 3, 10, 16, and 22 months.

(B) Quantification of BRN3A^{+} RGC numbers in aged WT and *Spp1*$^{-/-}$ mice (n = 8).

(C) BRN3A-labeled RGCs in WT and *Spp1*$^{-/-}$ mice after IOP elevation.

(D–F) Quantification of BRN3A^{+} RGC numbers after 1 month of elevated IOP (D), pattern ERG amplitude (E), and visual acuity (F) in WT and *Spp1*$^{-/-}$ mice after high IOP (n = 6).

(G) Total axon counts per nerve in WT and *Spp1*$^{-/-}$ mice after high IOP (n = 3).

(H) Correlation of cumulative IOP (cIOP) versus RGC density in WT and *Spp1*$^{-/-}$ mice after high IOP (n = 6).
(I) BRN3A-labeled RGCs in WT and *Spp1*$^{-/-}$ mice on days 3, 7, 14, and 21 after optic nerve crush (ONC).
(J) Quantification of BRN3A^{+} RGC numbers after ONC (n = 8).
The p values were determined by two-way ANOVA (B and J) or one-way ANOVA (D–G); *p < 0.05, **p < 0.01, ***p < 0.001. Data are mean ± SEM.

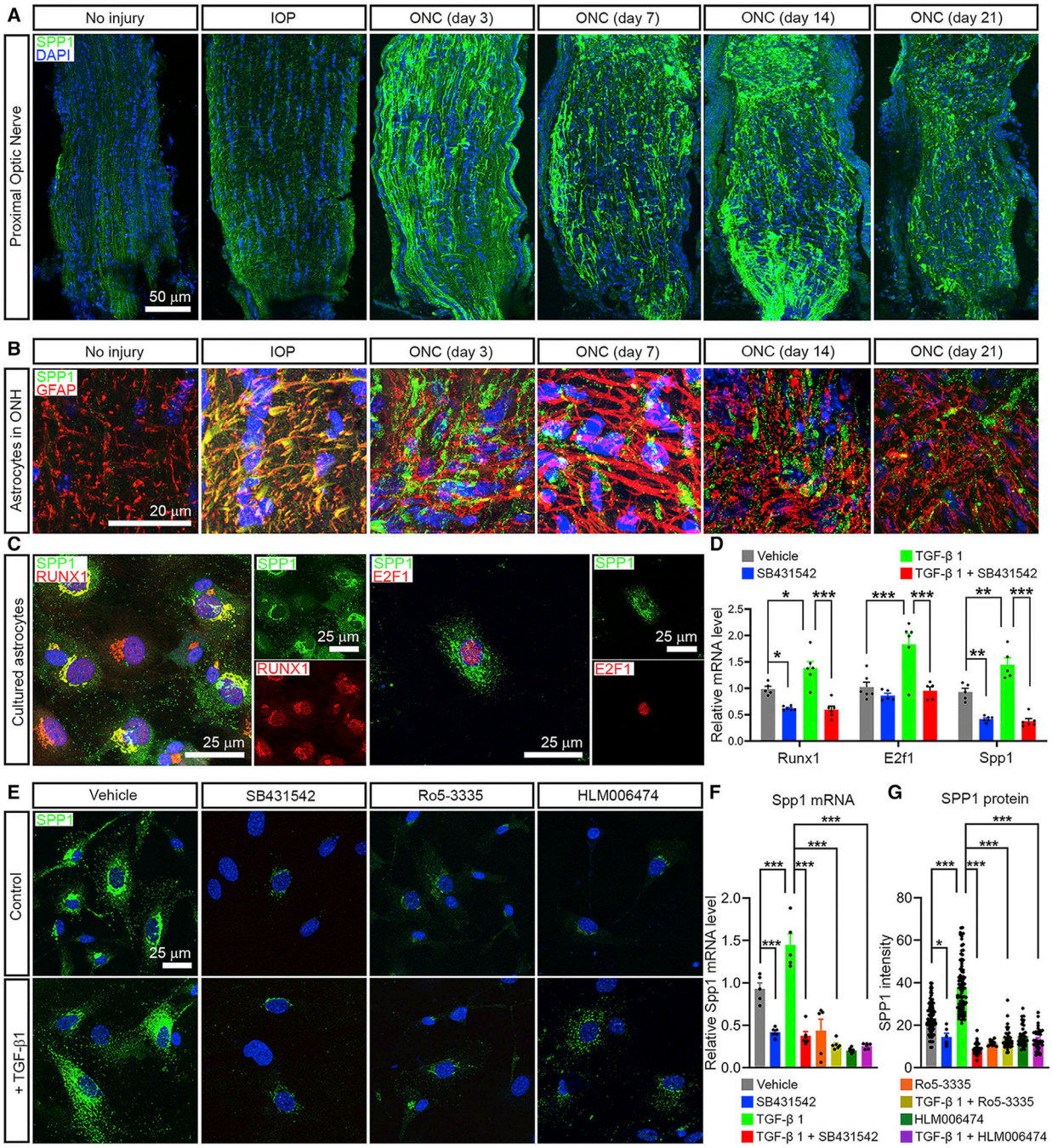

Figure 2. SPP1 is induced by the TGF-β1/TGFBR1/RUNX1/E2F1 signaling cascade in astrocytes

(A) SPP1 immunostaining in the proximal optic nerve under normal conditions (no injury), after high IOP, and after ONC.

(B) SPP1 immunostaining (green) in ONH astrocytes counterstained with GFAP (red) after high IOP and on days 3, 7, 14, and 21 after ONC.

(C) Co-expression of SPP1 with RUNX1 (left panels) and with E2F1 (right panels) in cultured astrocytes.

(D) Quantification of Runx1, E2f1, and Spp1 mRNA in cultured astrocytes when incubated with TGF-β1, the TGFβ1 receptor TGFBR1 blocker SB431542, and TGF-β1 plus SB431542 (n = 5–6).

(E) SPP1 immunostaining in cultured astrocytes treated with TGF-β1, SB431542, the RUNX1 antagonist Ro5-3335, the E2F1 antagonist HLM006474, and TGF-β1 plus SB431542, Ro5-3335, or HLM006474.

(F and G) Quantification of Spp1 mRNA (F) and protein (G) expression in cultured astrocytes treated with TGF-β1, SB431542, Ro5-3335, HLM006474, and TGF-β1 plus SB431542, Ro5-3335, or HLM006474 (n = 5–6 for mRNA, 6–110 for protein).

The p values were determined by two-way ANOVA (D) or one-way ANOVA (F and G); *p < 0.05, **p < 0.01, ***p < 0.001. Data represent mean ± SEM.

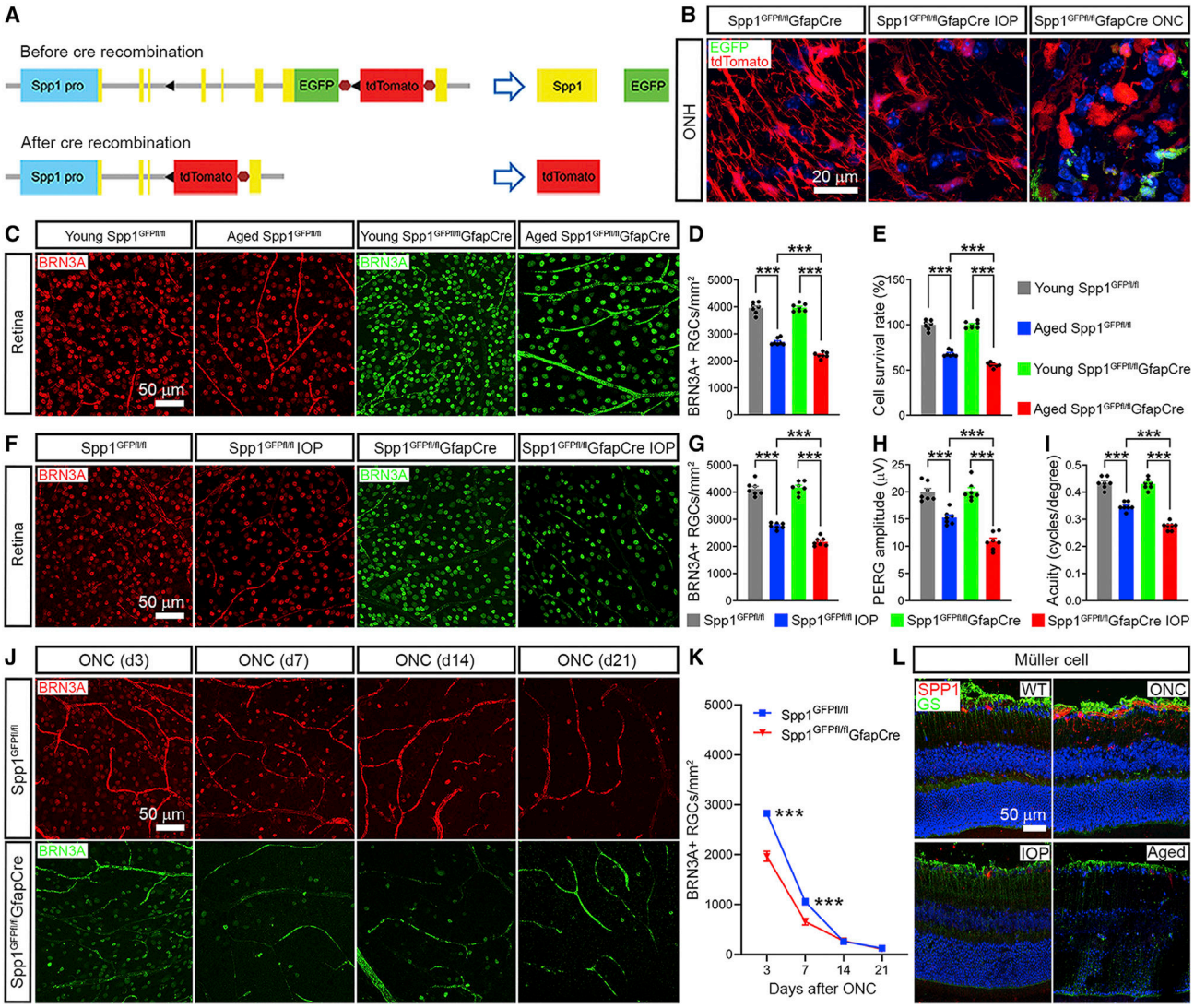

Figure 3. Astrocytic SPP1 deficiency aggravates RGCs loss and vision impairment in aging, glaucoma, and traumatic optic nerve injury

(A) Design of strain B6.Spp1$^{fl\text{-}EGFP\text{-}Stop\text{-}tdTomato}$ (Spp1$^{GFPfl/fl}$) before and after cre-mediated recombination.

(B) Validation of Spp1 conditional KO in ONH astrocytes in Spp1$^{GFPfl/fl}$GfapCre mice generated from Spp1$^{GFPfl/fl}$ crossed to Gfap-cre mice.

(C) BRN3A-labeled RGCs in young (3-month-old) and aged (16-month-old) Spp1$^{GFPfl/fl}$ and Spp1$^{GFPfl/fl}$GfapCre mice.

(D and E) Quantification of BRN3A^{+} RGC numbers (D) and cell survival rate (E) in aged Spp1$^{GFPfl/fl}$GfapCre mice, suggesting that astrocytic SPP1 deficiency accelerated age-dependent RGC loss (n = 7).

(F) BRN3A-labeled RGCs in Spp1$^{GFPfl/fl}$ and Spp1$^{GFPfl/fl}$GfapCre mice after high IOP.

(G–I) Quantification of BRN3A^{+} RGC numbers (G), pattern electroretinography (PERG) amplitude (H), and visual acuity (I) in Spp1$^{GFPfl/fl}$ and Spp1$^{GFPfl/fl}$GfapCre mice after high IOP (n = 7).

(J) BRN3A-labeled RGCs in Spp1$^{GFPfl/fl}$ and Spp1$^{GFPfl/fl}$GfapCre mice on days 3, 7, 14, and 21 after ONC.
(K) Quantification of BRN3A^{+} RGC numbers after ONC (n = 7).
(L) Immunostaining of SPP1 and glutamine synthetase (GS; a Müller cell marker) in retinas of C57BL/6 mice under normal conditions (no injury), after high IOP injury, after ONC injury, and in aging.
The p values were determined by one-way ANOVA (D, E, and G–I) or two-way ANOVA (K); ***$p < 0.001$. Data are mean ± SEM.

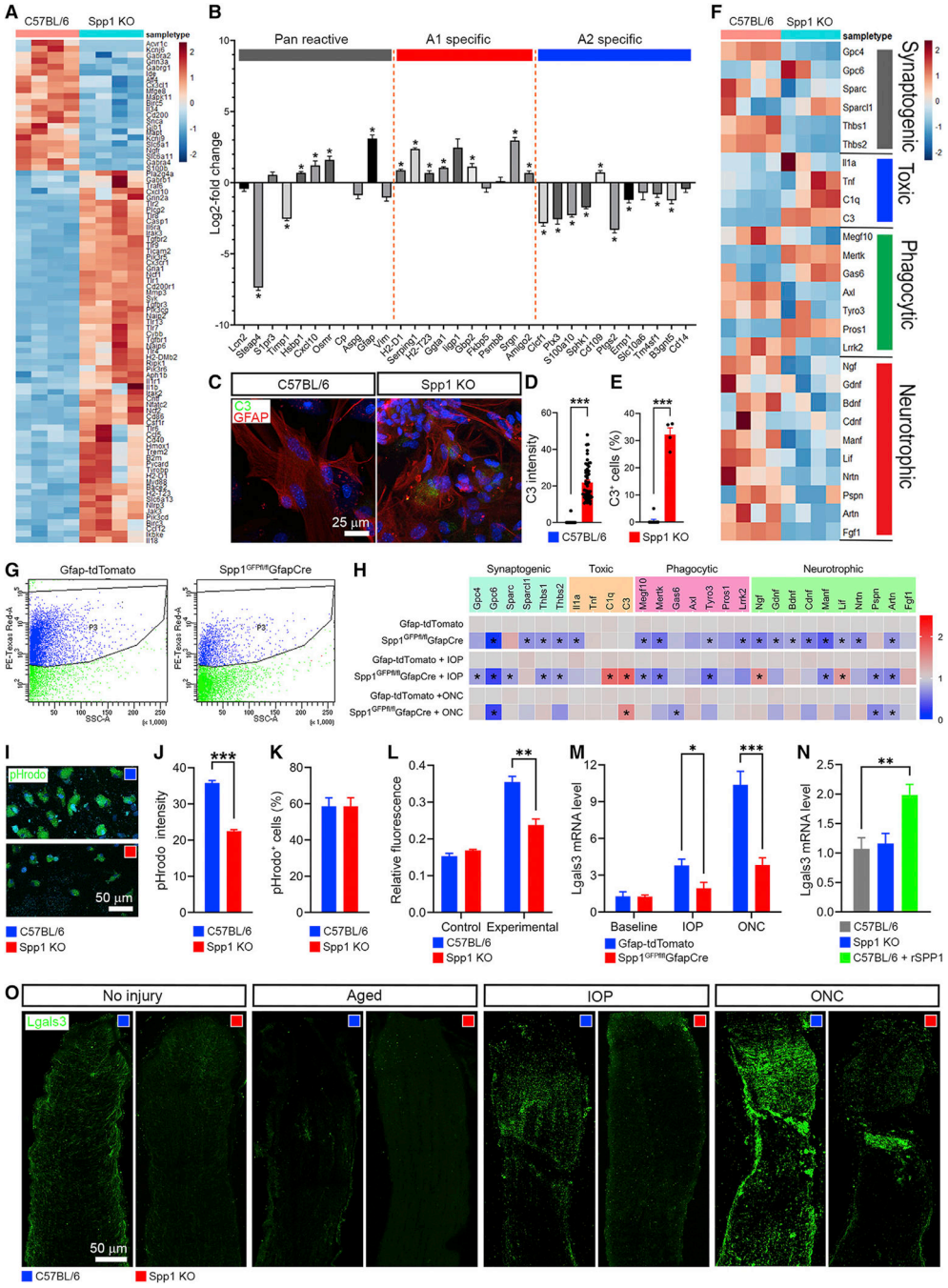

Figure 4. Spp1 deletion in astrocytes induces a neurotoxic state and impairs phagocytosis

(A) Genes involved in neuroinflammatory pathways were up-regulated in Spp1 KO astrocytes by RNA sequencing.

(B) Spp1 KO astrocytes showed a gene expression profile that was consistent with “A1”-reactive (i.e., neurotoxic) astrocytes by qPCR. Genes with $p < 0.05$ and absolute log2 (fold change) > 0.58 found by qPCR were considered differentially expressed (n = 4–6).

(C) Immunostaining of the neurotoxic marker C3 in Spp1 KO astrocytes.

(D and E) C3 fluorescence intensity (D, n = 43–51 cells/group) and $C3^+$ astrocytes percentage (E, n = 4–10) were increased in Spp1 KO astrocytes.
(F) Expression pattern of genes associated with other aspects of astrocyte function: synaptogenesis, neurotoxic factors, phagocytosis, and neurotrophic factors.
(G) $tdTomato^+$ astrocyte FACS from the ONH of Gfap-tdTomato and $Spp1^{GFPfl/fl}$GfapCre mice.
(H) mRNA levels of genes related to synaptogenesis, neurotoxic factors, phagocytosis, and neurotrophic factors in sorted ONH astrocytes from Gfap-tdTomato and $Spp1^{GFPfl/fl}$GfapCre mice under normal conditions, after high IOP, and after ONC (n = 5–6). The pairwise comparisons are between the Cre^- ($SPP1^+$ astrocytes in Gfap-tdTomato) and Cre^+ ($SPP1^-$ astrocytes in $Spp1^{GFPfl/fl}$GfapCre).
(I) Visualization of phagocytic activity by pHrodo particles in Spp1 KO astrocytes.
(J) Quantification of pHrodo particle fluorescence intensity in astrocytes by confocal microscopy (n = 87–123 cells/group).
(K) Percentages of $pHrodo^+$ astrocytes show no difference in phagocytosis ratio between Spp1 KO and C57BL/6 astrocytes (n = 5).
(L) Quantification of pHrodo particle relative fluorescence in astrocytes by spectrophotometry (n = 4).
(M) Quantification of Lgals3 mRNA in sorted ONH astrocytes from Gfap-tdTomato and from $Spp1^{GFPfl/fl}$GfapCre mice under baseline conditions, after high IOP, and after ONC (n = 6).
(N) Quantification of Lgals3 mRNA in cultured C57BL/6, Spp1 KO, and rSPP1-treated astrocytes.
(O) Lgals3 immunostaining in the proximal optic nerve under normal conditions (no injury), aged conditions, after high IOP, and after ONC.
The p values were determined by unpaired two-tailed t test (B, D, E, and J), multiple unpaired t test (H), two-way ANOVA (L and M), or one-way ANOVA (N); $*p < 0.05$, $**p < 0.01$, $***p < 0.001$. Data are mean ± SEM.

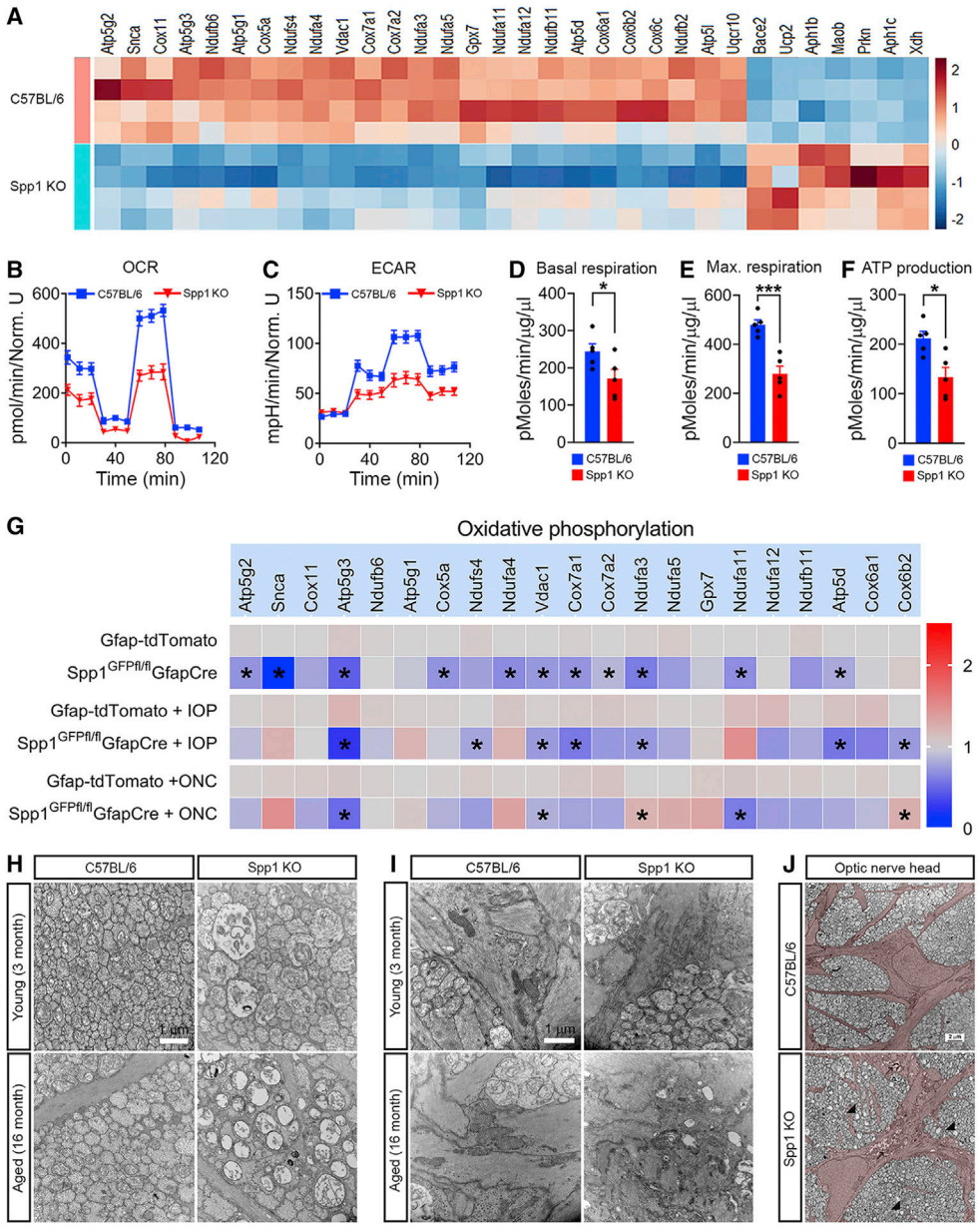

Figure 5. Astrocytic SPP1 promotes mitochondrial function

(A) Heatmap of oxidative phosphorylation genes in cultured Spp1 KO astrocytes by RNA sequencing analysis.

(B–F) Quantification of normalized oxygen consumption rate (OCR; B), extracellular acidification rate (ECAR; C), basal respiration (D), maximal respiration (E), and ATP production (F), showing a decrease in cultured Spp1 KO astrocytes compared with C57BL/6 astrocytes (n = 5).

(G) Expression of genes involved in oxidative phosphorylation shows down-regulation in sorted ONH astrocytes from Spp1$^{GFPfl/fl}$GfapCre and Gfap-tdTomato mice under normal conditions (no injury), after high IOP, and after ONC (n = 6).

(H and I) Transmission electron microscopy images of axonal mitochondria (H) and astrocytic mitochondria (I) in the optic nerve in young and aged C57BL/6 and Spp1 KO mice.

(J) Electron microscopy of the unmyelinated segment of optic nerves from C57BL/6 and Spp1 KO animals, showing mitochondria with few cristae in the axons of RGCs (arrowheads) and accumulation of partially degraded mitochondria in astrocytes (arrows). Astrocytes are false colored in red (representative TEM images were chosen from 4 Spp1 KO and 18 C57BL/6 mice).

The p values were determined by unpaired two-tailed t test (D–F) or multiple unpaired t test (G); *$p < 0.05$, ***$p < 0.001$. Data are mean ± SEM.

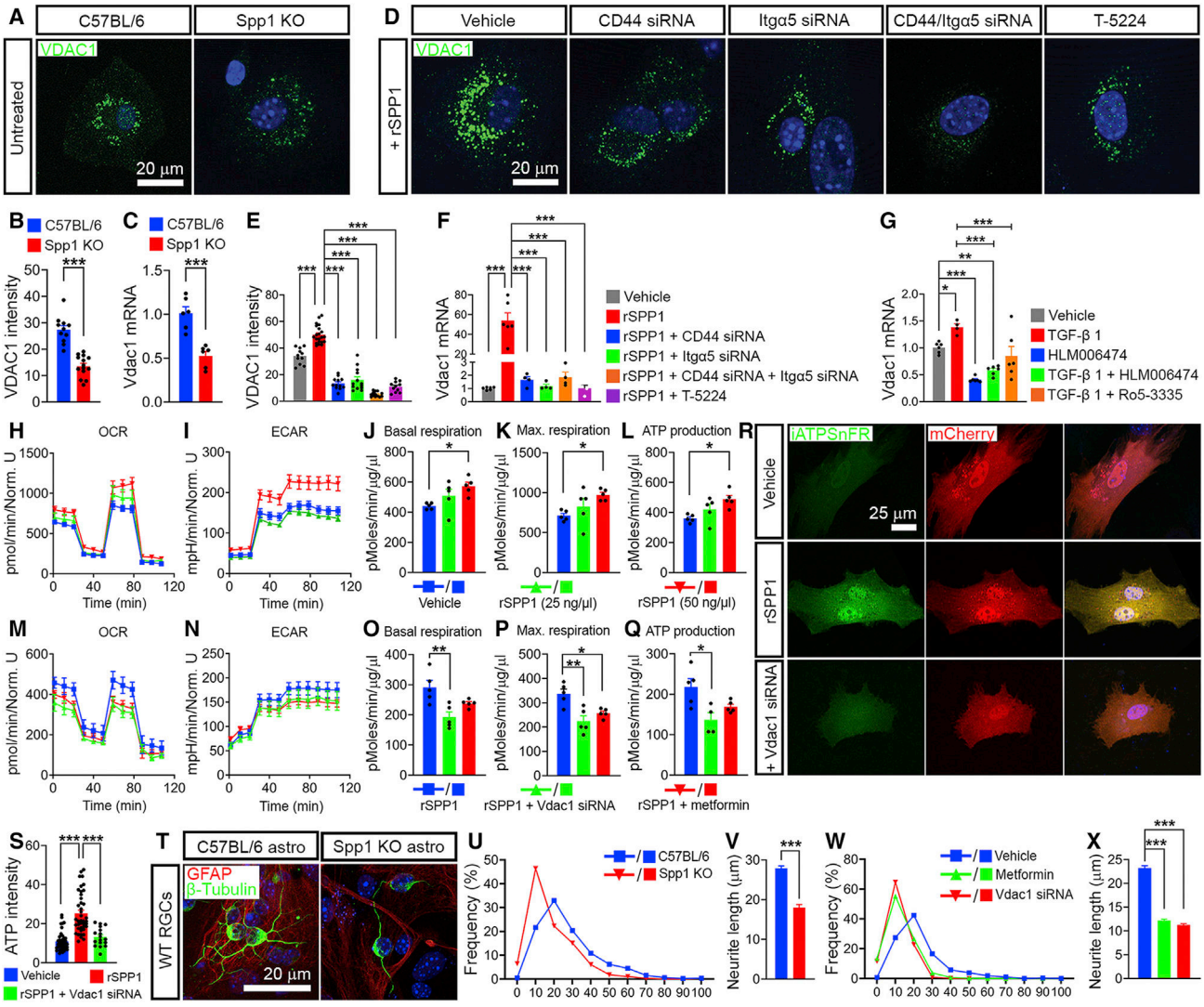

Figure 6. Astrocytic SPP1 induces mitochondrial VDAC1 expression and promotes mitochondrial function

(A) VDAC1 immunostaining in cultured C57BL/6 and Spp1 KO astrocytes.

(B and C) Down-regulation of Vdac1 protein (B) and mRNA (C) in Spp1 KO astrocytes (n = 11–14 cells/group for protein, n = 6/group for mRNA).

(D) VDAC1 immunostaining in cultured C57BL/6 astrocytes treated with rSPP1 and rSPP1 plus CD44 siRNA, Itgα5 siRNA, or the AP1 inhibitor T-5224.

(E and F) Quantification of VDAC1 protein (E) and mRNA (F) level in cultured C57BL/6 astrocytes treated with rSPP1 and rSPP1 plus CD44 siRNA, Itgα5 siRNA, or the AP1 inhibitor T-5224 (n = 11–21 cells/group for protein, n = 4–6/group for mRNA).

(G) Vdac1 mRNA expression was moderately up-regulated by TGF-β1/RUNX1/E2F1 signaling (n = 4–6).

(H–L) rSPP1 led to a dose-dependent increase in normalized OCR (H), ECAR (I), basal respiration (J), maximal respiration (K), and ATP production (L) in astrocytes (n = 5).

(M–Q) Knockdown of VDAC1 with siRNA or inhibition with metformin prevented an rSPP1-induced increase in normalized OCR (M), ECAR (N), basal respiration (O), maximal respiration (P), and ATP production (Q) (n = 4–5).

(R) Visualization of cytosolic ATP by transfection of the plasmid encoding the ATP sensor iATPsnFR and mCherry into astrocytes treated with rSPP1 or rSPP1 plus Vdac1 siRNA.

(S) Quantification of the ATP sensor iATPsnFR fluorescence intensity in astrocytes in (R) (n = 17–42 cells/group).

(T) WT RGCs from C57BL/6 mice were grown in co-culture with C57BL/6 or Spp1 KO astrocytes. Shown is visualization of RGCs and astrocytes by immunostaining of β-tubulin and GFAP.

(U and V) Scholl analysis of branching patterns of RGCs (U) and quantification of RGC total process length (V) when co-cultured with C57BL/6 and Spp1 KO astrocytes (n = 278–776 cells/group).

(W and X) Scholl analysis of branching patterns of RGCs (W) and quantification of RGCs total process length (X) when growing on C57BL/6 astrocytes on day 2 after Vdac1 knockdown with siRNA or inhibition with metformin (n = 673–961 cells/group).

The p values were determined by unpaired two-tailed t test (B, C, and V) or one-way ANOVA (E–G, J–L, O–Q, S, and X); *$p < 0.05$, **$p < 0.01$, ***$p < 0.001$. Data are mean ± SEM.

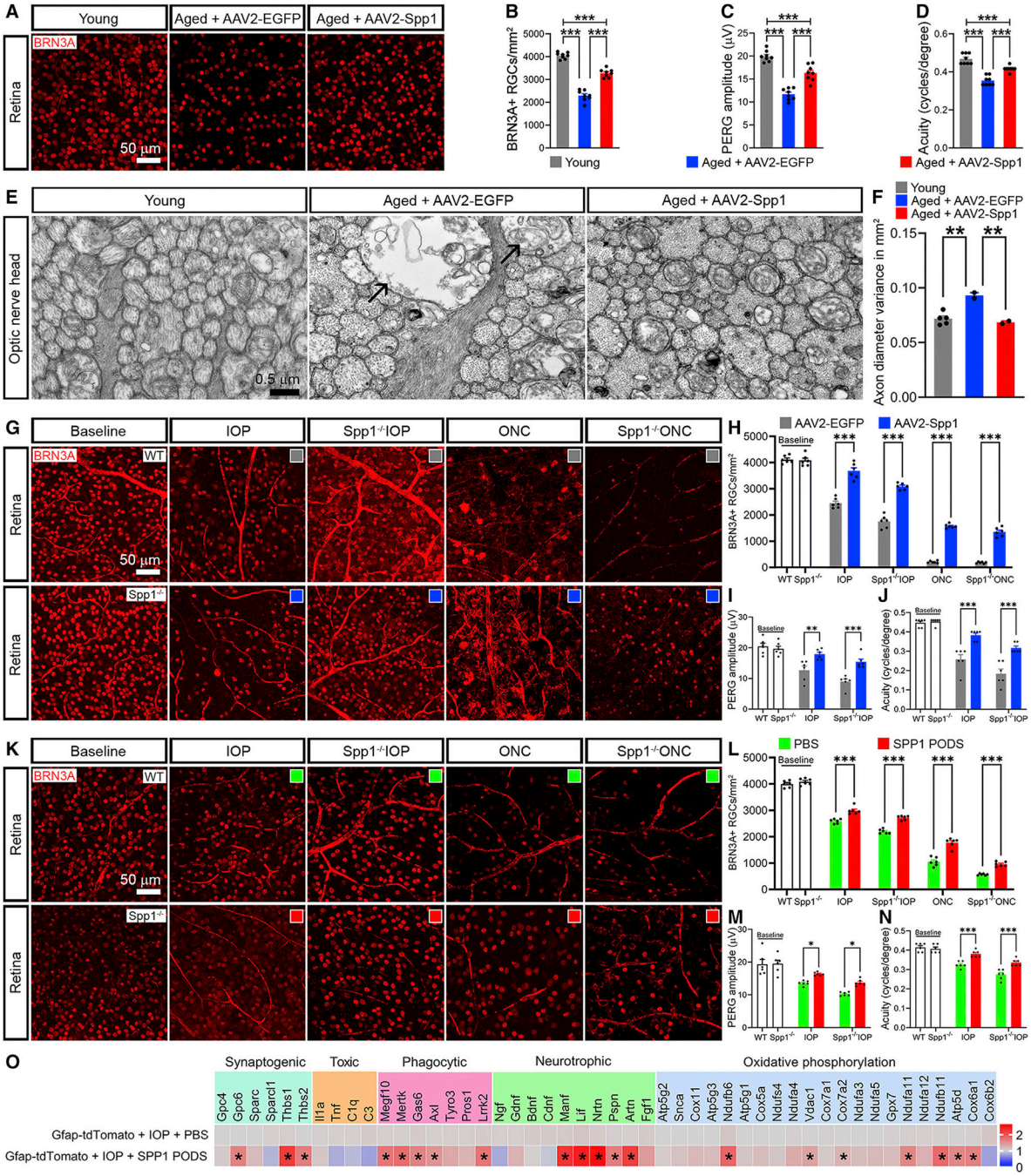

Figure 7. SPP1 overexpression prevents RGCs loss and preserves vision in aging, glaucoma, and traumatic optic injury

(A) BRN3A-labeled RGCs in young (4-month-old) and aged (16-month-old) WT mice treated with AAV2-Spp1 and AAV2-EGFP for 12 months.

(B–D) Quantification of BRN3A^{+} RGCs (B), PERG amplitude (C), and visual acuity (D) in aged WT mice with SPP1 overexpression. AAV2-driven SPP1 overexpression inhibited RGC loss, PERG impairment, and vision decline in aged mice (n = 8).

(E) Transmission electron microscopy images of axons in the optic nerve in aged WT mice treated with AAV2-Spp1. Arrows point to enlarged axons with pale axoplasm that are more typically found in aged animals.

(F) Quantification of axon diameter variance, a morphological sign of aging in the optic nerve. SPP1 overexpression resulted in a morphology similar to that of young mice (n = 2–5).

(G) BRN3A-labeled RGCs in WT and *Spp1*$^{-/-}$ mice treated with AAV2-Spp1 (blue square) and AAV2-EGFP (gray square) and followed by high IOP and ONC. Under baseline conditions (no injury), WT and *Spp1*$^{-/-}$ mice were not treated with AAV2.

(H–J) Quantification of BRN3A^{+} RGC numbers (H), PERG amplitude (I), and visual acuity (J) in WT and *Spp1*$^{-/-}$ mice with SPP1 overexpression, suggesting that AAV2-driven SPP1 overexpression inhibited RGC loss and restored vision in glaucoma and ONC mice (n = 6).

(K) BRN3A-labeled RGCs in WT and *Spp1*$^{-/-}$ mice treated with SPP1 PODS (red square) and PBS (green square) and followed by high IOP and ONC. Under baseline conditions (no injury), WT and *Spp1*$^{-/-}$ mice were naive.

(L–N) Quantification of BRN3A^{+} RGCs (L), PERG amplitude (M), and visual acuity (N) in WT and *Spp1*$^{-/-}$ mice treated with SPP1 PODS, showing that SPP1 PODS inhibited RGCs loss and vision decline in mice with high IOP and ONC injury (n = 6).

(O) mRNA levels of genes related to synaptogenesis, neurotoxic factors, phagocytosis, neurotrophic factors, and oxidative phosphorylation in sorted ONH astrocytes from Gfap-tdTomato mice treated with SPP1 PODS, followed by high IOP (n = 4–6).

The p values were determined by one-way ANOVA (B–D and F), two-way ANOVA (H–J and L–N), or multiple unpaired t test (O); *p < 0.05, **p < 0.01, ***p < 0.001. Data are mean ± SEM.

KEY RESOURCES TABLE

REAGENT or RESOURCE	SOURCE	IDENTIFIER
Antibodies		
Rabbit anti-Recoverin	Chemicon	Cat# AB5585; AB_2253622
Rabbit anti-PKCα	MyBioSource	Cat# MBS9405449;
Rabbit anti-Calbindin	Sigma-Aldrich	Cat# ABN2192;
Goat anti-ChAT	Chemicon	Cat# AB144P; AB_2079751
Peanut Agglutinin (PNA)	Vector Laboratories	Cat# FL-1071;AB_2315097
Mouse anti-Brdu	Sigma-Aldrich	Cat# B2531; RRID: AB_476793
Mouse anti-Brn3a	Millipore	Cat# MAB1585; RRID: AB_94166
Rat anit-C3	GeneTex	Cat# GTX11862; RRID: AB_367355
Chicken anti-GFAP	Abcam	Cat# ab4674; RRID: AB_304558
Rabbit anti-E2F1	Novus Biologicals	Cat# NBP2-56716;
Mouse anti-Neurofilament H (SMI32)	BioLegend	Cat# 801701; RRID: AB_2564642
Rabbit anti-Runx1	LSBio	Cat# LS-B13948
Rat anti-Galectin-3 (Lgals3)	Cedarlane	Cat# CL8942AP
Mouse anti-Glutamine Synthetase (GS)	Abcam	Cat# ab64613
Goat anti-Spp1 (full-length)	R&D Systems	Cat# AF808; RRID: AB_2194992
Rabbit anti-Spp1 (secretory)	Immuno-Biological Laboratories	Cat# 18621; RRID: AB_2341381
Rabbit anti-Vdac1	Abcam	Cat# ab15895; RRID: AB_2214787
Bacterial and virus strains		
AAV2-Spp1-EGFP	This study	N/A
AAV2-EGFP	This study	N/A
Biological samples		
Mouse eye tissue	Mouse strain is listed in the “Experimental Models: Organisms/ Strains”	N/A
C57BL/6 astrocytes	This study	N/A
Spp1 KO astrocytes	This study	N/A
C57BL/6 RGCs	This study	N/A
Chemicals, peptides, and recombinant proteins		
TGF-β 1	R&D Systems	Cat# 7666-MB/CF
SB431542 (TGF-β 1 receptor inhibitor)	Tocris Bioscience	Cat# 1614
RO5-3335 (Runx1 inhibitor)	Tocris Bioscience	Cat# 4694
HLM006474(E2F1 inhibitor)	Tocris Bioscience	Cat# 5283
T-5224 (AP-1 inhibitor)	APExBIO	Cat# B4664
Metformin (Vdac1 inhibitor)	Sigma-Aldrich	Cat# D150959
rSPP1	R&D Systems	Cat# 441-OP/CF
Brdu	Abcam	Cat# ab142567

REAGENT or RESOURCE	SOURCE	IDENTIFIER
CD44 siRNA	Thermo Fisher Scientific	Cat# 165814
Integrin alpha 5 siRNA	Thermo Fisher Scientific	Cat#67718
Vdac1 siRNA	Thermo Fisher Scientific	Cat# 187532
Silencer® Negative Control #1 siRNA	Thermo Fisher Scientific	Cat# AM4611
SPP1PODS	Cell Guidance Systems	Cat# PPH319-250
Oligomycin (ATP synthase inhibitor)	Millipore	Cat#495455
FCCP (carbonyl cyanide 4-(trifluoromethoxy) phenylhydrazone), (mitochondrial oxidative phosphorylation uncoupler)	Sigma-Aldrich	Cat# C2920
Rotenone (mitochondrial electron transport chain inhibitor)	Sigma-Aldrich	Cat# R8875
Antimycin A (mitochondrial electron transport chain inhibitor)	Sigma-Aldrich	Cat# A8674
Deposited data		
RNA-seq raw data (Spp1 KO)	This study	GSE174522
RNA-seq raw data (SB431542, Ro5-3335 and HLM006474)	This study	GSE174523
Code	This study	https://github.com/TCJakobs/SPP1_astrocytes
TEM microphotographs	This study	Harvard Dataverse (http://dataverse.harvard.edu/); Young Spp1 KO, https://dataverse.harvard.edu/dataset.xhtml?persistentId=doi:10.7910/DVN/BBWY1Z; Old Spp1 KO, https://dataverse.harvard.edu/dataset.xhtml?persistentId=doi:10.7910/DVN/M0UQOI; Old C57BL/6 treated with AAV2-EGFP, https://dataverse.harvard.edu/dataset.xhtml?persistentId=doi:10.7910/DVN/77G0G0; Old C57BL/6 treated with AAV2-Spp1, https://dataverse.harvard.edu/dataset.xhtml?persistentId=doi:10.7910/DVN/SXOOLV
Experimental models: Organisms/strains		
Mouse: C57BL/6J (WT)	Jackson Laboratory	Cat#000664
Mouse: B6.129S6(Cg)-Spp1^{tm1Blh}/J	Jackson Laboratory	Cat#004936
Mouse: B6.Spp1$^{fl\text{-}EGFP\text{-}stop\text{-}tdTomato}$	Produced by Cyagen	N/A
Mouse: B6.Cg-Tg(Gfap-cre)77.6Mvs/2J	Jackson Laboratory	Cat#024098
Mouse: B6.Cg-Gt(ROSA)26Sor$^{tm14(CAG\text{-}tdTomato)Hze}$/J	Jackson Laboratory	Cat#007914
Oligonucleotides		
Primers used for mouse genotyping	This study	See Table S1
Primers used for qRT-PCR	This study	See Table S1
Recombinant DNA		
GfaABC1D-cyto-Ruby3-iATPSnFR1.0	Addgene	Cat# 102554
Software and algorithms		
GraphPad Prism 8	https://www.graphpad.com/	RRID: SCR_002798

REAGENT or RESOURCE	SOURCE	IDENTIFIER
Adobe Photoshop CS6	https://www.adobe.com/products/photoshop.html	RRID: SCR_014199
Fiji	https://fiji.sc/	RRID: SCR_002285
RStudio	https://www.rstudio.com/	RRID: SCR_000432
Matlab	https://www.mathworks.com/products/matlab	RRID: SCR_001622